

# On Similarity Transformation Problems: Globally Optimal Results and Applications

Jin Wu, Chaoqun Wang, Chong Li, Yi Jiang, Chengxi Zhang, Yulong Huang, *Senior Member, IEEE*,

Yuhua Qi, Bohuan Xue, Jianhao Jiao, Rui Fan, and Wei Zhang , *Senior Member, IEEE*

**Abstract**—Similarity transformation problems are important in robotic instrumentation and computer vision based measurements since in many cases the information of visually observed scene scale is unknown and must be restored for accurate 3-dimensional reconstruction. In existing solvers, the scale is often considered as a scalar, i.e., isotropic, which may be invalid for anisotropic-scale setups. This paper exploits some mathematical coincidences that will lead to efficient solution to these problems. Possible further applications also include hand-eye calibration and structure-from-motion. We revisit pose estimation problems within the framework of similarity transformation, the one that considers scale-stretching, rotation and translation simultaneously. Two major problems are taken into account, i.e., the scale-stretching point-cloud registration and perspective-n-points (PnP). It has been found out that these two problems are quite similar. Moreover, we solve the anisotropic-scale registration problem that is important and is a remaining unsolved one in previous literatures. To compute the globally optimal solution of these non-convex problems, algebraic solution is obtained to compute all local minima using computationally efficient methods. The designed algorithm is deployed for robotic-arm pose estimation. We also extend the algorithm for solving the problem of robust magnetometer calibration. Visual pose experiments verify the superiority of the proposed method compared with representatives, including P3P, Lambda-Twist P3P and EPnP, which can be reproduced by repository in <https://github.com/zarathustr/APnP>.

**Index Terms**—Pose estimation, similarity transform, point-cloud registration, perspective-n-points (PnP), absolute orientation

Manuscript received 12th November, 2023; revised 26th March, 2024 and 14th May, 2024; accepted 3rd June, 2024. This article was recommended for publication by Associate Editor X X and Editor D. Liu upon evaluation of the reviewers' comments. This work was supported in part by the National Natural Science Foundation of China under Grant No. 62103237. (*Corresponding authors: Chaoqun Wang, Wei Zhang*).

J. Wu, B. Xue, J. Jiao, and Wei Zhang are with Department of Electronic and Computer Engineering, Hong Kong University of Science and Technology, Hong Kong, China (E-mail: eeweiz@ust.hk).

C. Wang is with School of Control Science and Engineering, Shandong University, Jinan 250061, China (E-mail: zychaoqun@gmail.com).

C. Li is with Department of Automation and Measurement, Ocean University of China, Qingdao, China (e-mail: cz10047@auburn.edu).

Y. Jiang is with the Department of Electrical Engineering, City University of Hong Kong, Hong Kong, China (E-mail: yjian22@cityu.edu.hk).

C. Zhang is with School of Internet of Things, Jiangnan University, Wuxi, China (e-mail: dongfangxy@163.com).

Y. Qi is with School of Systems Science and Engineering, Sun Yat-Sen University, China (E-mail: qiylh8@mail.sysu.edu.cn)

Y. Huang is with the Department of Automation, Harbin Engineering University, Harbin 150001, China (E-mail: heuedu@163.com).

R. Fan is with College of Electronics and Information Engineering, Tongji University, Shanghai, China (E-mail: rui.fan@ieee.org).

Color versions of one or more of the figures in this article are available online at <http://ieeexplore.ieee.org>.

Digital Object Identifier 10.1109/TIM.20XX.XXXX

## NOMENCLATURE

$\ \cdot\ $	Euclidean norm
$X^T$	Transpose of matrix $X$
$x_{\times}$	Skew symmetric matrix of vector $x$
$q$	Unit attitude quaternion
$I$	Identity matrix of proper size
$0$	Zeros matrix of proper size
$\mathbb{R}^n$	Real $n$ -dimensional vector space
$\mathbb{R}^{n \times m}$	Real $n \times m$ matrix space
$\mathbb{Z}$	Non-negative integer space
$\mathbb{R}_+^n$	Real $n$ -dimensional vector space with positive entries
$\mathcal{N}(\gamma, \Sigma)$	Normal distribution with mean of $\gamma$ and covariance of $\Sigma$
$SO(n)$	$n$ -dimensional special orthogonal group
$SE(n)$	$n$ -dimensional special Euclidean group

## I. INTRODUCTION

### A. Motivation and Related Work

ACCURATE robotic navigation and mapping require precise pose estimation from visual measurements, including images and point-cloud information [1], [2]. Among well-developed methods, the point-cloud registration (PCR) and perspective-n-points (PnP) are two major categories for estimating relative or absolute poses. The point-cloud registration aims to determine the relative pose between successive 3-D/3-D point-cloud measurements. The PnP solves the camera pose by the correspondence between 2-D image points and 3-D world points. Registration-based methods can also be shifted to solving vision-based calibration problems [3], [4]. In these two methods, the determination of scale is vital, as it links the estimates to the geometry of the real world. Therefore, current research efforts are mainly devoted to obtaining accurate estimate of scale, rotation and translation simultaneously.

Extensive efforts have been paid to solving PCR and PnP problems. Markley and Arun proposed solvers for point-to-point registration early back to 1980s, respectively [5], [6]. The kernel problem of PCR is the determination of point correspondences between two point sets to be registered. This motivates the idea of iterative closest point (ICP) that was proposed in 1990s [7]–[9]. The ICP is challenging, non-convex and NP-hard, since the sizes of two point sets are not identical. In many registration problems, the scale factor is always unknown because of different measurement principles and unsatisfactory calibration. Horn solves this scale-stretching

registration in [10], [11] by analytical results. This was later introduced to the ICP for refined scale-factor determination [12]. For the PnP problem, the scale is the depth of the pixel that is significant to the size of 3-D reconstruction. Early methods use direct linear transform (DLT) [13] by vectorizing rotation matrix. An approximate pose solution will be obtained and will be refined by taking the nearest rotation (orthonormalization) into account [14], [15]. The perspective-3-points (P3P) solves the PnP problem by taking three points of them and verify the solution via an external fourth point [16]. These methods are simple and computationally efficient, but will suffer from large errors when the input measurements are noisy. The efficient PnP (EPnP) algorithm solves the method in a least-square manner with singular value decomposition [17]. There are other variants of PCR, e.g., the ones using various metrics of point-to-plane [18] and point-to-line [19] ones, which are not the objective of this paper. Some other methods of PnP solve the problem by considering the scale as a nonlinear function of attitude and translation [20], [21]. And the new problem is no longer a similarity transformation problem, which needs extensive efforts for solving the nonlinear optimization. We also do not discuss them in this paper. In other words, this paper targets at solving the problem analytically to a maximum extent. To this end, we must face the following challenges behind the related research:

- *Challenge 1 - Scale Matters:* We also notice that, following the research trend introduced above, there are still remaining problems in the field. First, the connection between these problems are not very clear. Furthermore, previous methods only considers the isotropic scale in estimation. However, in real world scenarios, usually practitioners will encounter anisotropic-scale point-cloud registration (APCR) problems. For instance, if we consider registration of point sets measured by two different laser scanners, the scale may not be the same. Currently, there is a trend in point-cloud registration that merges the anisotropic concerns into the original one [22]. However, the anisotropic-scale registration problem is still not solved completely. It is currently challenging, as in the conclusion of [12], it has been pointed out that the anisotropic-scale registration is much harder than the isotropic one.
- *Challenge 2 - Convergence is Tough:* Although there has been further studies on the anisotropic registration by Du et al. [23] and Li et al. [24], the results show that there exists local minima in their algorithm and satisfactory initial guess must be obtained to guarantee the global convergence, which may be false in terms of high outlier rate. This problem continuously exists in further related works [25], [26], which highly limits the practical performance.
- *Challenge 3 - More Applications Meet Registration:* In [27], it is inferred that the anisotropic-scale registration is highly related to sensor calibration issues, which are important in inertial navigation and robotics. But the problem is so non-convex and only approximate optimization can be solved. Therefore, it will be a little

bit difficult to transfer existing results of isotropic-scale registration to another. This paper aims to solve these remaining issues that are important to the community. Theoretical and experimental results support our new findings. With contributions to be revealed in the next sub-section, this paper treats another challenge, i.e., the data association problem, as a well-solved one. The reason is that the data association problem, sometimes also referred to as the correspondence matching problem, is completely different one, which receives popularity from diverse communities. In this way, this work will only use some mature data association techniques in experimental validation stage.

## B. Contributions

In this paper, we revisit these problems by unifying them as the similarity transformation problem. The contributions of this paper are summarized as:

- 1) First, through theoretical analysis, we show that scale-stretching PCR and PnP are very similar. In this way, a simple eigenvalue solution is designed that unifies them together.
- 2) We extend the isotropic-scale registration to anisotropic-scale one. The new problem is non-convex. Therefore, approximate and globally optimal solutions are derived to solve this challenging problem. The proposed globally optimal method is convergence-free while initial-value-free, leading to the fact that it is efficient and deterministic.
- 3) The developed theory is transferred to solve not only the anisotropic-scale registration and PnP, but also it helps solve the problem of magnetometer calibration, where a point-to-surface registration scheme is proposed.

## C. Outline

The remainder of the paper is organized as follows: Section II-B to Section II-D first introduce the details of several similarity transformation problems to be studied. Local and globally optimal solutions are then presented in Section III. Two experimental applications, results and comparisons are shown in Section IV. Finally, concluding remarks are drawn in Section V.

# II. SIMILARITY TRANSFORMATION PROBLEMS

## A. Transformations

Some notations are defined in the Nomenclature in the beginning of this paper. Rotation matrices distribute on the manifold of  $n$ -dimensional special orthogonal group such that  $SO(n) := \{\mathbf{R} \in \mathbb{R}^{n \times n} | \mathbf{R}^T \mathbf{R} = \mathbf{I}, \det(\mathbf{R}) = +1\}$ . The special Euclidean group complements  $SO(n)$  with an additional translation vector:

$$SE(n) := \left\{ \left( \begin{array}{c|c} \mathbf{R} & \mathbf{t} \\ \mathbf{0} & 1 \end{array} \right) \middle| \mathbf{R} \in SO(n), \mathbf{t} \in \mathbb{R}^n \right\} \quad (1)$$

in which  $\mathbf{0}$  denotes a zero matrix with adequate size. When the scale factor is considered, the similarity transformation group is

$$\text{Sim}(n) := \left\{ \begin{pmatrix} s\mathbf{R} & \mathbf{t} \\ \mathbf{0} & 1 \end{pmatrix} \middle| s \in \mathbb{R}, \mathbf{R} \in \text{SO}(n), \mathbf{t} \in \mathbb{R}^n \right\}.$$

In this paper,  $\text{Sim}(n)$  is extended to  $\text{SIM}(n)$ , that characterizes the scale factor in an anisotropic manner

$$\text{SIM}(n) := \left\{ \begin{pmatrix} \mathbf{SR} & \mathbf{t} \\ \mathbf{0} & 1 \end{pmatrix} \middle| \mathbf{S} \in \text{diag}(\mathbb{R}_+^n), \mathbf{R} \in \text{SO}(n), \mathbf{t} \in \mathbb{R}^n \right\}$$

where  $\mathbb{R}_+^n$  stands for the set of n-D real positive vectors. For 3-dimensional cases, rotation can be parameterized with unit quaternion, say  $\mathbf{q} = (q_0, q_1, q_2, q_3)^\top$ . Rotation matrix  $\mathbf{R}$  is quadratically represented in terms of elements of  $\mathbf{q}$ , so the negative quaternion  $-\mathbf{q}$  represents the same rotation as  $\mathbf{R}$ . Quaternion has the only constraint of unitary norm thus it is more convenient in optimization problems. Note that, quaternion is not the simplest formulation for 3-dimensional rotation parameterization. For any  $n$ -dimensional rotation matrix  $\mathbf{R}$ , it has related Lie algebra  $\xi$  such that  $\mathbf{R} = \exp(\xi_\times)$ , in which  $\xi_\times$  denotes a mapping from  $\mathbb{R}^{n(n-1)/2}$  to  $\mathbb{R}^{n \times n}$ . However, there are infinity many  $\xi$  correspond to  $\mathbf{R}$  since  $\xi$  is periodic. Thus even for 3-dimensional case, the computation of Jacobian may be truncated using limited elements of expansion of  $\exp(\xi_\times)$ . The introduction of Lie algebra simplifies the number of variables for identifying rotation but brings more nonlinearity. As a consequence, this paper uses the unit quaternion as a kernel tool for solution of optimization problems.

### B. Problem I: Scale-Stretching 3-D Registration

What we are concerning the most in the remainder of this paper includes the scale-stretching PCR and PnP problems. Given two 3-dimensional point sets  $\{\mathcal{B}\}$  and  $\{\mathcal{R}\}$ , the scale-stretching PCR (SPCR) aligns the two sets together by solving the following absolute orientation problem

$$\arg \min_{s \in \mathbb{R}, \mathbf{R} \in \text{SO}(3), \mathbf{t} \in \mathbb{R}^3} \mathcal{L}_{\text{SPCR}} = \sum_{i=1}^{\mathcal{N}} \|\mathbf{b}_i - s\mathbf{R}\mathbf{r}_i - \mathbf{t}\|^2 \quad (2)$$

in which  $\mathbf{b}_i \in \{\mathcal{B}\}$  and  $\mathbf{r}_i \in \{\mathcal{R}\}$  are points from two sets. Note that here we assume that the correspondences between  $\{\mathcal{B}\}$  and  $\{\mathcal{R}\}$  have been fixed. The scale-stretching PCR deals with the registration problem on  $\text{Sim}(3)$ . Scale-stretching phenomenon usually comes from devices with different scale factors. Thus it is frequently required for 3-D/3-D alignment between multiple point cloud measurements from laser scanners.

### C. Problem II: Perspective-n-Points

The PnP aims to solve the pose estimation problem between the undistorted 2-D points in the image plane and corresponding 3-D points in the world frame. Given image coordinates  $\mathbf{u}_i \in \mathbb{R}^2$  for  $i = 1, 2, \dots, \mathcal{N}$  and their related 3-D world points  $\mathbf{v} \in \mathbb{R}^3$  for  $i = 1, 2, \dots, \mathcal{N}$ , one would like to achieve the following perspective transformation

$$s(\mathbf{u}_i^\top, 1)^\top = \mathbf{K}(\mathbf{R}\mathbf{v}_i + \mathbf{t}). \quad (3)$$

where  $\mathbf{K} \in \mathbb{R}^{3 \times 3}$  is an affine calibration matrix (intrinsic) accounting for the focal lengths and central points in horizontal and vertical directions respectively. Denoting  $\mathbf{b}_i = (\mathbf{u}_i^\top, 1)^\top$  and  $\mathbf{r}_i = \mathbf{v}_i$ , it is able for us to construct the optimization of

$$\arg \min_{s \in \mathbb{R}, \mathbf{R} \in \text{SO}(3), \mathbf{t} \in \mathbb{R}^3} \mathcal{L}_{\text{PnP}} = \sum_{i=1}^{\mathcal{N}} \|\mathbf{s}\mathbf{b}_i - \mathbf{R}\mathbf{r}_i - \mathbf{t}\|^2. \quad (4)$$

Here,  $s$ ,  $\mathbf{R}$  and  $\mathbf{t}$  form a transformation on  $\text{Sim}(3)$ . Normally,  $s$  is not independent of  $\mathbf{R}$ , because from (3), one can conclude from the last line that  $s$  is in nonlinear form of  $\mathbf{R}$  and  $\mathbf{t}$ . Therefore, the essential way for solving highly accurate PnP relies on optimization of bundle adjustment (BA). However, to obtain a good initial guess of BA,  $s$  can be treated independently from  $\mathbf{R}$  and  $\mathbf{t}$ , such is a common practice in popular solvers like EPnP [17].

### D. Problem III: Anisotropic-Scale Registration

In registration with anisotropic scale factors, the following nonlinear least square problem is considered

$$\arg \min_{\mathbf{R} \in \text{SO}(3), \mathbf{t} \in \mathbb{R}^3, \mathbf{S} \in \text{diag}(\mathbb{R}_+^3)} \mathcal{L}_{\text{APCR}} = \sum_{i=1}^{\mathcal{N}} \|\mathbf{b}_i - \mathbf{S}\mathbf{R}\mathbf{r}_i - \mathbf{t}\|^2 \quad (5)$$

in which  $\mathbf{b}_i$  and  $\mathbf{r}_i$  are  $i$ -th correspondence point pair from two point sets  $\{\mathcal{B}\}$  and  $\{\mathcal{R}\}$  respectively.  $\mathbf{R}$  denotes the rotation matrix that distributes on the special orthogonal group  $\text{SO}(3)$  subject to the nonlinear constraints  $\mathbf{R}^\top \mathbf{R} = \mathbf{I}$ ,  $\det(\mathbf{R}) = 1$ .  $\mathbf{t}$  acts as a translation vector while  $\mathbf{S}$  contains three positive anisotropic scale factors such that  $\mathbf{S} = \text{diag}(s_1, s_2, s_3)$  with  $s_1, s_2, s_3$  being positive numbers in the real positive set  $\mathbb{R}_+$ . Here  $\mathbf{S}$ ,  $\mathbf{R}$  and  $\mathbf{t}$  constitute a transformation on  $\text{SIM}(3)$ . Previously, in [12], a scale-stretching ICP problem has been studied where  $\mathbf{S}$  degenerates to a scalar, that is exactly the scale-stretching registration problem stated above. The APCR problem is much more challenging than previous one as mentioned in the concluding remarks of [12], where strong coupling between  $\mathbf{S}$  and  $\mathbf{R}$  has been illustrated. Therefore, the problem is challenging in the aspect of globally optimal optimization solution.

## III. SOLUTIONS

### A. Scale-Stretching Registration and PnP

The elements of  $\mathbf{b}_i$  and  $\mathbf{r}_i$  are  $\mathbf{b}_i = (b_{i,1}, b_{i,2}, b_{i,3})^\top$  and  $\mathbf{r}_i = (r_{i,1}, r_{i,2}, r_{i,3})^\top$  respectively. (2) and (4) specify the target objective of the scale-stretching PCR and PnP. From these expressions, it is clear that the only difference is the location of  $s$ . In the following contents, we are going to show some algebraic results for solving these problems. Moreover, the two problems are eventually solved in a unified fashion.

The objective of PnP can be extended as

$$\mathcal{L}_{\text{PnP}} = \sum_{i=1}^{\mathcal{N}} (\mathbf{s}\mathbf{b}_i - \mathbf{R}\mathbf{r}_i - \mathbf{t})^\top (\mathbf{s}\mathbf{b}_i - \mathbf{R}\mathbf{r}_i - \mathbf{t}). \quad (6)$$

Introducing the unit quaternion  $\mathbf{q}$  for attitude parameterization of  $\mathbf{R}$ , the Lagrangian is

$$\tilde{\mathcal{L}}_{\text{PnP}} = \mathcal{L}_{\text{PnP}} + \lambda (\mathbf{q}^\top \mathbf{q} - 1) \quad (7)$$

where  $\lambda \in \mathbb{R}$  is the Lagrange multiplier. Here, a detailed relationship between a unit quaternion and a rotation matrix can be found in [28]. Then all local optimum occur at the place where the Jacobian is zero. To compute the Jacobian analytically, some previous results are invoked. The rotation matrix  $\mathbf{R} = (\mathbf{P}_1\mathbf{q}, \mathbf{P}_2\mathbf{q}, \mathbf{P}_3\mathbf{q})$  in which  $\mathbf{P}_1, \mathbf{P}_2$  and  $\mathbf{P}_3$  are linear matrix of  $\mathbf{q}$  [29], [30], thus

$$\mathbf{R}\mathbf{r}_i = (\mathbf{P}_1\mathbf{q}, \mathbf{P}_2\mathbf{q}, \mathbf{P}_3\mathbf{q}) \mathbf{r}_i = \sum_{j=1}^3 r_{i,j} \mathbf{P}_j \mathbf{q} \quad (8)$$

which gives

$$\partial \mathbf{b}_i^\top \mathbf{R} \mathbf{r}_i / \partial \mathbf{q} = \sum_{j=1}^3 r_{i,j} \mathbf{P}_j^\top \mathbf{b}_i = \sum_{j=1}^3 r_{i,j} \mathbf{M}_j(\mathbf{b}_i) \mathbf{q} \quad (9)$$

where  $\mathbf{M}_j$  matrix is linear in the form of  $\mathbf{b}_i$  (see [30]). In this way, the blocks of Jacobian are

$$\frac{\partial \tilde{\mathcal{L}}_{\text{PnP}}}{\partial \mathbf{q}} = 2\lambda \mathbf{q} - 2 \sum_{i=1}^{\mathcal{N}} \sum_{j=1}^3 r_{i,j} \mathbf{M}_j(\mathbf{b}_i) (\mathbf{s} \mathbf{b}_i - \mathbf{t}) \mathbf{q}, \quad (10)$$

$$\frac{\partial \tilde{\mathcal{L}}_{\text{PnP}}}{\partial \mathbf{t}} = 2\mathcal{N} \mathbf{t} - 2 \sum_{i=1}^{\mathcal{N}} \mathbf{s} \mathbf{b}_i - \mathbf{R} \mathbf{r}_i, \quad (11)$$

$$\frac{\partial \tilde{\mathcal{L}}_{\text{PnP}}}{\partial \mathbf{s}} = 2 \sum_{i=1}^{\mathcal{N}} \mathbf{b}_i^\top (\mathbf{s} \mathbf{b}_i - \mathbf{R} \mathbf{r}_i - \mathbf{t}). \quad (12)$$

The optimality meets  $\nabla \tilde{\mathcal{L}}_{\text{PnP}} = \mathbf{0}$ . Then one has

$$\mathbf{t} = \mathbf{s} \bar{\mathbf{b}} - \mathbf{R} \bar{\mathbf{r}}, \quad (13)$$

$$\lambda \mathbf{q} = \sum_{i=1}^{\mathcal{N}} \sum_{j=1}^3 r_{i,j} \mathbf{M}_j [s(\mathbf{b}_i - \bar{\mathbf{b}}) + \mathbf{R} \bar{\mathbf{r}}] \mathbf{q}, \quad (14)$$

$$\mathbf{s} = \left[ \sum_{i=1}^{\mathcal{N}} \mathbf{b}_i^\top \mathbf{R} (\mathbf{r}_i - \bar{\mathbf{r}}) \right] / \left[ \sum_{i=1}^{\mathcal{N}} \mathbf{b}_i^\top (\mathbf{b}_i - \bar{\mathbf{b}}) \right]. \quad (15)$$

Introducing the identities

$$\mathbf{P}_i^\top \mathbf{P}_i \mathbf{q} = \mathbf{q}, \quad (16)$$

$$(\mathbf{P}_i^\top \mathbf{P}_j + \mathbf{P}_j^\top \mathbf{P}_i) \mathbf{q} = \mathbf{0}, \quad (17)$$

the term  $\mathbf{M}_j(\mathbf{R} \bar{\mathbf{r}}) \mathbf{q}$  can be simplified to scaled form of  $\mathbf{q}$ , say  $\alpha \mathbf{q}$ . Therefore,  $\mathbf{q}$  will be solved via the following problem

$$\mathbf{s} \mathbf{W} \mathbf{q} = (\lambda - \alpha) \mathbf{q} \quad (18)$$

in which

$$\mathbf{W} = 1/\mathcal{N} \sum_{i=1}^{\mathcal{N}} \sum_{j=1}^3 r_{i,j} \mathbf{M}_j(\mathbf{b}_i - \bar{\mathbf{b}}). \quad (19)$$

Note that, for this problem,  $\mathbf{q}$  is an eigenvector of  $\mathbf{W}$  associated with the eigenvalue of  $(\lambda - \alpha)/s$ .  $\mathbf{W}$  is a  $4 \times 4$  symmetric matrix so there will be 4 real eigenvalues corresponding to 4 possible local minima. Inserting these 4 possible solutions of  $\mathbf{q}$  back into (13) gives 4 possible solutions of  $\mathbf{s}$ . The optimal set of solution is then obtained by checking the loss-function value  $\mathcal{L}_{\text{PnP}}$ . These techniques are similar for SPCR problem. The Lagrangian is

$$\tilde{\mathcal{L}}_{\text{SPCR}} = \mathcal{L}_{\text{SPCR}} + \lambda (\mathbf{q}^\top \mathbf{q} - 1). \quad (20)$$

We use the fact that  $\mathbf{R}$  can be decomposed into

$$\mathbf{R}^\top = (\mathbf{Q}_1 \mathbf{q}, \mathbf{Q}_2 \mathbf{q}, \mathbf{Q}_3 \mathbf{q}) \quad (21)$$

in which  $\mathbf{Q}_1, \mathbf{Q}_2, \mathbf{Q}_3$  are linear matrices of  $\mathbf{q}$ . The derivative of the loss function with respect to quaternion is

$$\frac{\partial \tilde{\mathcal{L}}_{\text{SPCR}}}{\partial \mathbf{q}} = 2\lambda \mathbf{q} - \left( \sum_{i=1}^{\mathcal{N}} \sum_{j=1}^3 s r_{i,j} \mathbf{M}_j [(\mathbf{b}_i - \bar{\mathbf{b}})] + r_{i,j} \mathbf{I} \right) \mathbf{q} \quad (22)$$

indicating that the solution is also an eigenvalue problem, like (18).

### B. Anisotropic-Scale Registration

For the anisotropic registration, from single-pair equation  $\mathbf{b}_i = \mathbf{S} \mathbf{R} \mathbf{r}_i + \mathbf{t}$ , one can conclude the averaged form as  $\bar{\mathbf{b}} = \mathbf{S} \mathbf{R} \bar{\mathbf{r}} + \mathbf{t}$ , that further gives a new optimization

$$\arg \min_{\mathbf{R} \in \text{SO}(3), \mathbf{S} \in \text{diag}(\mathbb{R}_+^3)} \mathcal{L}_{\text{APCR},1} = \sum_{i=1}^{\mathcal{N}} \left\| \tilde{\mathbf{b}}_i - \mathbf{S} \mathbf{R} \tilde{\mathbf{r}}_i \right\|^2 \quad (23)$$

which is decentralized one without translation  $\mathbf{t}$  with  $\tilde{\mathbf{b}}_i = \mathbf{b}_i - \bar{\mathbf{b}} = (b_{i,1}, b_{i,2}, b_{i,3})^\top$ ,  $\tilde{\mathbf{r}}_i = \mathbf{r}_i - \bar{\mathbf{r}} = (r_{i,1}, r_{i,2}, r_{i,3})^\top$ . Then the following norm-based optimization is constructed

$$\arg \min_{\mathbf{S} \in \text{diag}(\mathbb{R}_+^3)} \mathcal{L}_{\text{APCR},\mathbf{S}} = \sum_{i=1}^{\mathcal{N}} \left( \tilde{\mathbf{b}}_i^\top \mathbf{S}^{-2} \tilde{\mathbf{b}}_i - \tilde{\mathbf{r}}_i^\top \tilde{\mathbf{r}}_i \right)^2. \quad (24)$$

The Jacobian of  $\mathcal{L}_{\text{APCR},\mathbf{S}}$  is

$$\frac{\partial \mathcal{L}_{\text{APCR},\mathbf{S}}}{\partial \mathbf{s}} = 4 \sum_{i=1}^{\mathcal{N}} \begin{pmatrix} b_{i,1}^2 \beta / s_1^3 \\ b_{i,2}^2 \beta / s_2^3 \\ b_{i,3}^2 \beta / s_3^3 \end{pmatrix}. \quad (25)$$

in which  $\mathbf{s} = (s_1, s_2, s_3)^\top$  and  $\beta = (\|\tilde{\mathbf{r}}_i\|^2 - b_{i,1}^2/s_1^2 - b_{i,2}^2/s_2^2 - b_{i,3}^2/s_3^2)$ . To solve  $\mathbf{s}$ , the equation  $\partial \mathcal{L}_{\text{APCR},\mathbf{S}} / \partial \mathbf{s} = \mathbf{0}$  must be solved. This results in the following polynomial equation after simplification

$$\begin{cases} g_2 g_3 a_{11} + g_1 g_3 a_{12} + g_1 g_2 a_{13} + g_1 g_2 g_3 a_{14} = 0 \\ g_2 g_3 a_{21} + g_1 g_3 a_{22} + g_1 g_2 a_{23} + g_1 g_2 g_3 a_{24} = 0 \\ g_2 g_3 a_{31} + g_1 g_3 a_{32} + g_1 g_2 a_{33} + g_1 g_2 g_3 a_{34} = 0 \end{cases} \quad (26)$$

with  $g_1 = s_1^2, g_2 = s_2^2, g_3 = s_3^2$  and

$$\begin{aligned} a_{11} &= -\sum b_{i,1}^4, a_{12} = -\sum b_{i,1}^2 b_{i,2}^2, a_{13} = -\sum b_{i,1}^2 b_{i,3}^2, \\ a_{14} &= \sum b_{i,1}^2 \|\tilde{\mathbf{r}}_i\|^2, a_{21} = -\sum b_{i,1}^2 b_{i,2}^2, a_{22} = -\sum b_{i,2}^4, \\ a_{23} &= -\sum b_{i,2}^2 b_{i,3}^2, a_{24} = \sum b_{i,2}^2 \|\tilde{\mathbf{r}}_i\|^2, a_{31} = -\sum b_{i,1}^2 b_{i,3}^2, \\ a_{32} &= -\sum b_{i,2}^2 b_{i,3}^2, a_{33} = -\sum b_{i,3}^4, a_{34} = \sum b_{i,3}^2 \|\tilde{\mathbf{r}}_i\|^2. \end{aligned} \quad (27)$$

The closed-form solution to  $g_1, g_2, g_3$  is

$$g_1 = -G/G_1, g_2 = G/G_2, g_3 = -G/G_3 \quad (28)$$

where  $G = a_{11} a_{22} a_{33} - a_{11} a_{23} a_{32} - a_{12} a_{21} a_{33} + a_{12} a_{23} a_{31} + a_{13} a_{21} a_{32} - a_{13} a_{22} a_{31}$ ,  $G_1 = a_{12} a_{23} a_{34} - a_{12} a_{24} a_{33} - a_{13} a_{22} a_{34} + a_{13} a_{24} a_{32} + a_{14} a_{22} a_{33} - a_{14} a_{23} a_{32}$ ,  $G_2 = a_{11} a_{23} a_{34} - a_{11} a_{24} a_{33} - a_{13} a_{21} a_{34} + a_{13} a_{24} a_{31} + a_{14} a_{21} a_{33} - a_{14} a_{23} a_{31}$  and  $G_3 = a_{11} a_{22} a_{34} - a_{11} a_{24} a_{32} - a_{12} a_{21} a_{34} + a_{12} a_{24} a_{31} + a_{14} a_{21} a_{32} - a_{14} a_{22} a_{31}$ . Then  $\mathbf{s}$  can be obtained via

$$s_1 = \sqrt{g_1}, s_2 = \sqrt{g_2}, s_3 = \sqrt{g_3}. \quad (29)$$

It should be noticed that (24) only considers the norm constraint so the coupling between  $\mathbf{S}$  and  $\mathbf{R}$  is lost. Thus (29) is an approximate solution of  $\mathbf{s}$ .

Once an approximate set of scale factors has been found, inserting it back into (23) gives an approximate rotation estimate, say  $\mathbf{R}_0$ . This step can be achieved via either SVD [6] or eigen-decomposition (EIG) [7]. Using the approximate

scale  $S_0$ , the following equality for  $i$ -th vector pair can be achieved

$$\tilde{\mathbf{b}}_i = S_0 \tilde{S} \tilde{R} R_0 \tilde{\mathbf{r}}_i \quad (30)$$

where  $S_0 \tilde{S} = S$  and  $\tilde{R} R_0 = R$  are true values of scale and rotation.  $\tilde{S}$  and  $\tilde{R}$  are error states of scale and rotation respectively. By setting  $\mathbf{u}_i = S_0^{-1} \tilde{\mathbf{b}}_i$  and  $\mathbf{v}_i = R_0 \tilde{\mathbf{r}}_i$ , a new equivalent optimization for the error states can be established

$$\arg \min_{\tilde{R} \in \text{SO}(3), \tilde{S} \in \text{diag}(\mathbb{R}_+^3)} \sum_{i=1}^{\mathcal{N}} \left\| \mathbf{u}_i - \tilde{S} \tilde{R} \mathbf{v}_i \right\|^2 \quad (31)$$

which can be solved recursively via the formulae presented above. By repeating such construction over and over again, we gradually achieve the minimum. Note that  $\tilde{R}$  will eventually converge to identity matrix  $I$  but convergence rate will be quite slow for final iterations. To solve this problem efficiently, we consider  $\tilde{R}$  to be a small-angle rotation, which can be parameterized as  $R = I + \theta_{\times}$ , in which  $\theta = (\theta_1, \theta_2, \theta_3)^{\top}$  characterize small Euler angles and  $\theta_{\times}$  is its associated skew-symmetric matrix. Denoting  $\mathbf{x} = (\theta^{\top}, s^{\top})^{\top}$ , solving  $\mathbf{x}$  optimally is identical to find all roots by zeroing the Lagrangian derivative. Simplified polynomial system is given by (32), where  $h_{ij}$  are coefficient for the  $i$ -th equation's  $j$ -th monomial. Note that in this system, many coefficients can be omitted by reducing variables via the following equalities:

$$\begin{aligned} h_{12} &= -h_{11}, h_{21} = -h_{18}, h_{22} = h_{18}, h_{23} = h_{13}, h_{27} = h_{17}, \\ h_{28} &= h_{11}, h_{31} = h_{17}, h_{32} = -h_{17}, h_{33} = h_{14}, h_{34} = h_{24}, \\ h_{37} &= h_{18}, h_{38} = h_{11}, h_{42} = h_{24}, h_{43} = h_{13}, h_{44} = h_{14}, \\ h_{45} &= h_{25}, h_{46} = h_{35}, h_{47} = -2h_{18}, h_{48} = 2h_{17}, h_{49} = 2h_{11} \\ h_{52} &= h_{14}, h_{53} = h_{13}, h_{54} = h_{24}, h_{55} = h_{15}, h_{56} = h_{36}, \\ h_{57} &= 2h_{11}, h_{58} = -2h_{17}, h_{59} = 2h_{18}, h_{62} = h_{13}, h_{63} = h_{14}, \\ h_{64} &= h_{24}, h_{65} = h_{16}, h_{66} = h_{26}, h_{67} = -2h_{11}, h_{68} = 2h_{18} \end{aligned} \quad (33)$$

and  $h_{69} = 2h_{17}$ . Required coefficients are summarized in (34)

$$\begin{aligned} h_{11} &= \sum_{i=1}^{\mathcal{N}} v_{i,2} v_{i,3}, h_{13} = \sum_{i=1}^{\mathcal{N}} v_{i,3}^2, h_{14} = \sum_{i=1}^{\mathcal{N}} v_{i,2}^2, h_{15} = \sum_{i=1}^{\mathcal{N}} u_{i,2} v_{i,3}, \\ h_{16} &= -\sum_{i=1}^{\mathcal{N}} u_{i,3} v_{i,2}, h_{17} = -\sum_{i=1}^{\mathcal{N}} v_{i,1} v_{i,2}, h_{18} = -\sum_{i=1}^{\mathcal{N}} v_{i,1} v_{i,3}, \\ h_{24} &= \sum_{i=1}^{\mathcal{N}} v_{i,1}^2, h_{25} = -\sum_{i=1}^{\mathcal{N}} u_{i,1} v_{i,3}, h_{26} = \sum_{i=1}^{\mathcal{N}} u_{i,3} v_{i,1}, \\ h_{35} &= \sum_{i=1}^{\mathcal{N}} u_{i,1} v_{i,2}, h_{36} = -\sum_{i=1}^{\mathcal{N}} u_{i,2} v_{i,1}, h_{41} = -\sum_{i=1}^{\mathcal{N}} u_{i,1} v_{i,3} \end{aligned} \quad (34)$$

and  $h_{51} = -\sum_{i=1}^{\mathcal{N}} u_{i,2} v_{i,2}$ ,  $h_{61} = -\sum_{i=1}^{\mathcal{N}} u_{i,3} v_{i,3}$ . It should be noticed that from last three sub-equations of (32), one can directly solve  $s_1, s_2, s_3$  in terms of  $\theta_1, \theta_2, \theta_3$ , i.e.

$$\begin{aligned} s_1 &= -(h_{41} + h_{45}\theta_2 + h_{46}\theta_3) / \\ &\quad (h_{43}\theta_2^2 + h_{49}\theta_2\theta_3 + h_{47}\theta_2 + h_{44}\theta_3^2 + h_{48}\theta_3 + h_{42}) \\ s_2 &= -(h_{51} + h_{55}\theta_1 + h_{56}\theta_3) / \\ &\quad (h_{53}\theta_1^2 + h_{59}\theta_1\theta_3 + h_{57}\theta_1 + h_{54}\theta_3^2 + h_{58}\theta_3 + h_{52}) \\ s_3 &= -(h_{61} + h_{65}\theta_1 + h_{66}\theta_2) / \\ &\quad (h_{63}\theta_1^2 + h_{69}\theta_1\theta_2 + h_{67}\theta_1 + h_{64}\theta_2^2 + h_{68}\theta_2 + h_{62}). \end{aligned} \quad (35)$$

Thus replacing  $s_1, s_2, s_3$  with (35) produces a system with unknowns of  $\theta_1, \theta_2, \theta_3$  only. The transformed system is a little bit sophisticated. Related monomials are shown in (36). To solve this nonlinear polynomial system, we may use the Gröbner-basis method. Gröbner bases are common properties of a certain polynomial system. They actually represent a reduced form of original polynomials so they are easier to be solved via variable elimination. However, Gröbner-basis method is not applicable for solving this system since the reduced Gröbner bases are too complicated so that evaluating these bases consumes much more time even than numerical optimizers. Therefore, to efficiently solve the new system containing only elements of  $\theta$ , a linear equation is appended:  $H = 1 + \theta_1 + \theta_2 + \theta_3$ , which is a linear combination of first-order monomials  $\{1, \theta_1, \theta_2, \theta_3\}$ . Since the magnitude of  $\theta$  is small, high-order terms will be very tiny. In this way, we depart  $\zeta_{\theta}$  into two sub-groups  $\zeta_1$  and  $\zeta_2$ , where  $\zeta_1$  contains all terms with orders of no more than 3 and  $\zeta_2$  consists of the remainder. Stacking all coefficient of original polynomials of  $\theta$  forms the Macaulay matrix  $\mathcal{M}$  such that

$$\mathcal{M} \zeta_{\theta} = \mathbf{0}. \quad (37)$$

However, after extending  $H$  to the original system, the  $H$  is not zero in general. Denoting the new Macaulay matrix as  $\bar{\mathcal{M}}$ , using  $H$  as the first extended equation of the new polynomial, we can write  $\bar{\mathcal{M}}$  as

$$\bar{\mathcal{M}} = \begin{pmatrix} \bar{\mathcal{M}}_1 & \bar{\mathcal{M}}_2 \\ \bar{\mathcal{M}}_3 & \bar{\mathcal{M}}_4 \end{pmatrix} \quad (38)$$

$$(H \zeta_1^{\top}, \mathbf{0})^{\top} = \bar{\mathcal{M}} (\zeta_1^{\top}, \zeta_2^{\top})^{\top}. \quad (39)$$

Using the identity of Schur complement, we have

$$\mathcal{K} = \bar{\mathcal{M}}_1 - \bar{\mathcal{M}}_2 \bar{\mathcal{M}}_4^{-1} \bar{\mathcal{M}}_3. \quad (40)$$

So it follows that

$$\mathcal{F} \zeta_1 = H \zeta_1 \quad (41)$$

$$\begin{cases} h_{15}s_2 + h_{16}s_3 + h_{11}s_2^2 + h_{12}s_3^2 + h_{13}s_2^2\theta_1 + h_{14}s_3^2\theta_1 + h_{17}s_3^2\theta_2 + h_{18}s_2^2\theta_3 = 0 \\ h_{25}s_1 + h_{26}s_3 + h_{21}s_1^2 + h_{22}s_3^2 + h_{23}s_1^2\theta_2 + h_{24}s_3^2\theta_2 + h_{27}s_3^2\theta_1 + h_{28}s_1^2\theta_3 = 0 \\ h_{35}s_1 + h_{36}s_2 + h_{31}s_1^2 + h_{32}s_2^2 + h_{33}s_1^2\theta_3 + h_{34}s_2^2\theta_3 + h_{37}s_2^2\theta_1 + h_{38}s_1^2\theta_2 = 0 \\ h_{41} + h_{42}s_1 + h_{45}\theta_2 + h_{46}\theta_3 + h_{43}s_1\theta_2^2 + h_{44}s_1\theta_3^2 + h_{47}s_1\theta_2 + h_{48}s_1\theta_3 + h_{49}s_1\theta_2\theta_3 = 0 \\ h_{51} + h_{52}s_2 + h_{55}\theta_1 + h_{56}\theta_3 + h_{53}s_2\theta_1^2 + h_{54}s_2\theta_3^2 + h_{57}s_2\theta_1 + h_{58}s_2\theta_3 + h_{59}s_2\theta_1\theta_3 = 0 \\ h_{61} + h_{62}s_3 + h_{65}\theta_1 + h_{66}\theta_2 + h_{63}s_3\theta_1^2 + h_{64}s_3\theta_2^2 + h_{67}s_3\theta_1 + h_{68}s_3\theta_2 + h_{69}s_3\theta_1\theta_2 = 0 \end{cases} \quad (32)$$

$$\begin{aligned} \zeta_{\theta}^{\top} &= \{\theta_1^{\kappa_1} \theta_2^{\kappa_2} \theta_3^{\kappa_3} | \kappa_1, \kappa_2, \kappa_3 \in \mathbb{Z}_+\} \\ &= \left( 1, \theta_1, \theta_1^4, \theta_1^5, \theta_1^6, \theta_1^7, \theta_1^8, \theta_1^9, \theta_1^{10}, \theta_1^{11}, \theta_1^{12}, \theta_1^{13}, \theta_1^{14}, \theta_1^{15}, \theta_1^{16}, \theta_1^{17}, \theta_1^{18}, \theta_1^{19}, \theta_1^{20}, \theta_1^{21}, \theta_1^{22}, \theta_1^{23}, \theta_1^{24}, \theta_1^{25}, \theta_1^{26}, \theta_1^{27}, \theta_1^{28}, \theta_1^{29}, \theta_1^{30}, \theta_1^{31}, \theta_1^{32}, \theta_1^{33}, \theta_1^{34}, \theta_1^{35}, \theta_1^{36}, \theta_1^{37}, \theta_1^{38}, \theta_1^{39}, \theta_1^{40}, \theta_1^{41}, \theta_1^{42}, \theta_1^{43}, \theta_1^{44}, \theta_1^{45}, \theta_1^{46}, \theta_1^{47}, \theta_1^{48}, \theta_1^{49}, \theta_1^{50}, \theta_1^{51}, \theta_1^{52}, \theta_1^{53}, \theta_1^{54}, \theta_1^{55}, \theta_1^{56}, \theta_1^{57}, \theta_1^{58}, \theta_1^{59}, \theta_1^{60}, \theta_1^{61}, \theta_1^{62}, \theta_1^{63}, \theta_1^{64}, \theta_1^{65}, \theta_1^{66}, \theta_1^{67}, \theta_1^{68}, \theta_1^{69}, \theta_1^{70}, \theta_1^{71}, \theta_1^{72}, \theta_1^{73}, \theta_1^{74}, \theta_1^{75}, \theta_1^{76}, \theta_1^{77}, \theta_1^{78}, \theta_1^{79}, \theta_1^{80}, \theta_1^{81}, \theta_1^{82}, \theta_1^{83}, \theta_1^{84}, \theta_1^{85}, \theta_1^{86}, \theta_1^{87}, \theta_1^{88}, \theta_1^{89}, \theta_1^{90}, \theta_1^{91}, \theta_1^{92}, \theta_1^{93}, \theta_1^{94}, \theta_1^{95}, \theta_1^{96}, \theta_1^{97}, \theta_1^{98}, \theta_1^{99}, \theta_1^{100} \right) \end{aligned} \quad (36)$$

namely  $\zeta_1$  is the eigenvector of  $\mathcal{F}$  associated with eigenvalue  $H$ . In this way, all 27 eigenvectors of  $\mathcal{F}$  can be obtained. Not all of these 27 eigenvectors are real. Then selecting the real vectors and inserting them back to the loss function value, the global optimal solution will be obtained. Since the eigen-decomposition is highly numerical stable, the proposed method is also numerical stable.

#### IV. EXPERIMENTAL RESULTS

In this section, the experimental results from various sensors are reported. The proposed method has been applied to these cases where comparisons with representatives are systematically conducted. In all these experiments, the data association has been performed using k-d tree, which is easy-to-implement and classical.

##### A. Synthetic Evaluation: Comparisons with Existing Anisotropic Registration Methods

We replicate the anisotropic registration algorithms in [23]–[25]. These three methods all belong to the iterative algorithms which need a good initial guess to converge to the global minimum. We simulate randomly sampled point cloud data from the Stanford Bunny model [31]. We sample 50 cases with 5000 points to conduct registration. For each cases, first, 100 initial guess values are generated randomly for convergence analysis. For reference and transformed point pairs, the point numbers are consistent, i.e., there will be no data association challenges in this test. Then, we conduct another test using initial guess values provided in the original works (marked as Author-Given). The registration success rates are averaged and summarized in Table I. Seen from the results, since the pro-

TABLE I

SUCCESS RATES OF DIFFERENT ANISOTROPIC REGISTRATION METHODS

Initial	Du et al. [23]	Li et al. [24]	Chen et al. [25]	Proposed Global
Random	14.686%	18.922%	16.815%	100%
Author-Given	74.238%	63.401%	78.736%	100%

posed method is globally optimal, the method is free of initial-value selection and iterations. However, other representatives are all iterative. Thus the performance is largely dependent on the quality of initial guess. Although all these methods provide their respective initial value computing strategy in their works, they are not always leading to satisfactory registration results. This shows that our method is much more reliable and deterministic compared to these existing ones. We also

show anisotropic registration results of several open models. We utilize the *frog*<sup>1</sup> model and the *armadillo*<sup>2</sup> model for validation, whose standard models are shown in Fig. 1. The standard models are downsampled to high resolution point clouds. Gaussian noises with covariance of  $\Sigma = 10^{-2}m^2$  are added to the models, denoting a typical noisy sensor specification for modern 3-D LiDARs. The scale factors for two different models are emulated as 2.5 and 0.45 respectively. In these tests, rotation matrices, and translation vectors are generated randomly as ground truth. The evaluated registration results with estimated correspondences are shown in Fig. 2 and Fig. 3.

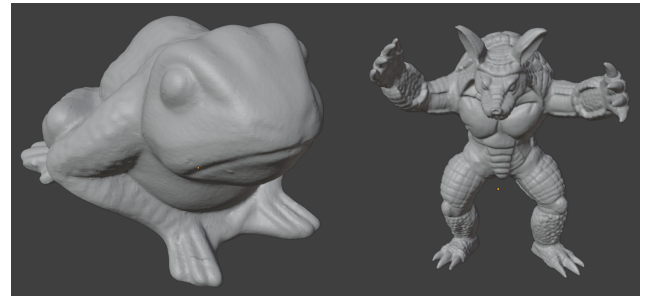


Fig. 1. The utilized standard models for accuracy comparisons of 3-D anisotropic registration methods.

Some representative candidates are employed for comparisons. We show the registration accuracy results for *frog* model in Fig. 4 and Fig. 5, with statistics shown in Table II. The error metrics are:

$$\begin{aligned} \mathcal{E}_{\text{rot}} &= \arccos \frac{\text{tr}(\mathbf{R}^{\top} \mathbf{R}_{\text{true}}) - 1}{2} \\ \mathcal{E}_{\text{trans}} &= \|\mathbf{t} - \mathbf{t}_{\text{true}}\| \end{aligned} \quad (42)$$

The results indicate that the proposed method achieves best rotation and translation accuracy in these tests. As shown in correspondences estimated previously, we may see that the proposed method can generate highly accurate point correspondences given noisy point cloud pairs. This shows that the method would be capable of estimating accurate poses encountering data with outliers.

##### B. Application I: Accurate PnP Camera Pose

When conducting dynamic grasping tasks with a dynamic camera, the camera needs to understand the pose of the robotic

<sup>1</sup><http://visionair.ge.imati.cnr.it/ontologies/shapes>

<sup>2</sup><https://graphics.stanford.edu/data/3Dscanrep>

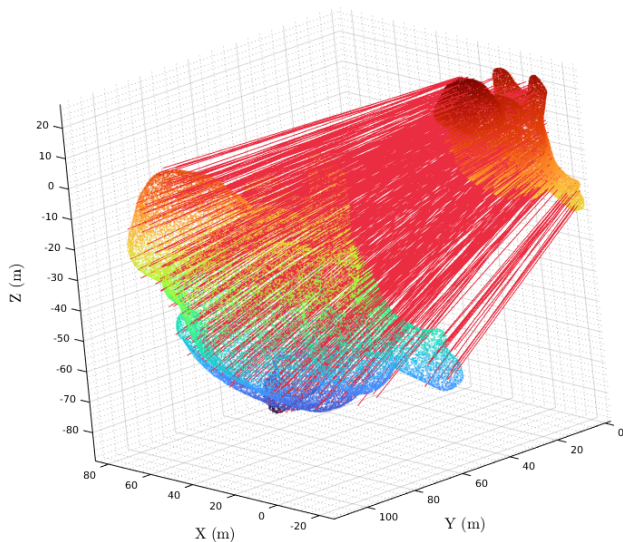


Fig. 2. The registration results with the proposed anisotropic scale estimation of the noisy frog models with estimated inlier correspondences (marked in red).

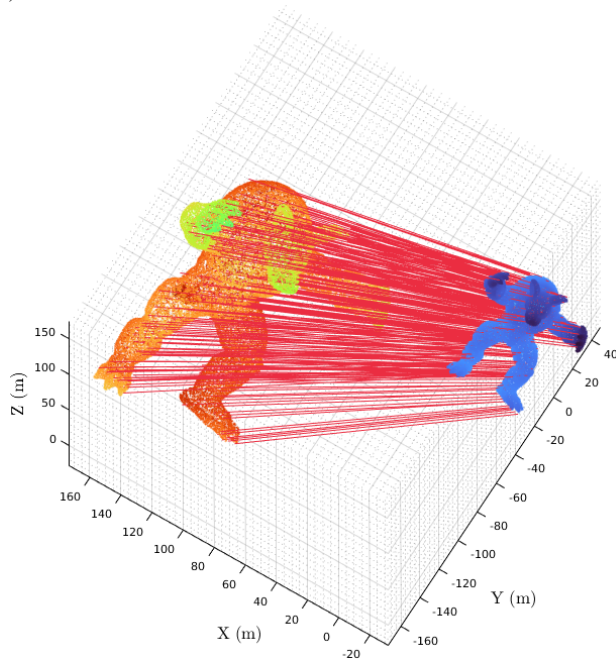


Fig. 3. The registration results with the proposed anisotropic scale estimation of the noisy armadillo models with estimated inlier correspondences (marked in red).

gripper in real-time. This requires accurate perception of the gripper pose by visual correspondences. In our platform shown in Fig. 6, there is a gripper installed on a 6-degree-of-freedom (6-DOF) robotic manipulator. There is a 4x4 mini chessboard pattern attached to the robotic gripper using standard printing. A dynamically moving ZED-M stereo camera gazes at the pattern on the gripper, so that the motion of the gripper can be inspected. To compute the relative camera pose (left camera) with respect to this mini gripper pattern, we implement the P3P [16], EPnP [17], Lambda-Twist P3P<sup>3</sup> [32] and our proposed

<sup>3</sup><https://github.com/midjji/lambdatwist-p3p>

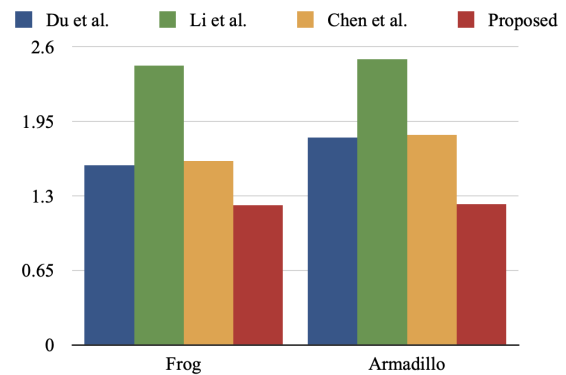


Fig. 4. Rotation errors of the proposed method with representative methods. The unit is degree.

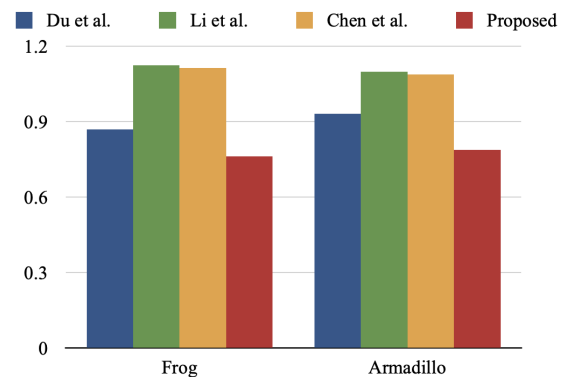


Fig. 5. Translation errors of the proposed method with representative methods. The unit is meters.

solution (18) for comparisons. The intrinsic calibration is obtained using MATLAB calibration toolbox, i.e. method of Dr. Zhengyou Zhang [33]. The corners of the pattern are extracted using the histogram method in [34]. Since the pattern is dark, direct corner extraction is trivial. We track the pattern using the fast correlation filter proposed in [35]. The trust region of the tracked area is used as the image for chessboard recognition and corner extraction (see Fig. 7). When implementing P3P method, we use the random sample consensus (RANSAC) to select the best fourth point for verified pose. After evaluation of each algorithm, the pose solution is refined by the same Quasi-Newton nonlinear optimizer by converting  $q$  to its Lie algebra  $\xi$ . The algorithms are evaluated via the averaged loss function value

$$\mathcal{L}_{\text{PnP,mean}} = \mathcal{L}_{\text{PnP}} / \mathcal{N} \quad (43)$$

in (4). We use this metric because this is a mean quality value, which is proportional to the reprojection error. We name the proposed method as the algebraic PnP (APnP). The loss function values of various methods in a single experiment are shown respectively in Fig. 8, Fig. 9 and Fig. 10.

The PnP reprojection errors are evaluated according to estimates given by various algorithms, whose snapshot is presented in Fig. 11. The root mean squared reprojection errors of various algorithms in pixels are presented in Table III. We use different markers to represent the projected corners from various algorithms. Among these projected

TABLE II  
ROTATION AND TRANSLATION ERRORS FOR ANISOTROPIC REGISTRATIONS USING DIFFERENT METHODS (FROG/ARMADILLO)

Methods	Rotation Error (°)	Translation Error (m)
Du et al. [23]	1.567/1.808	0.869/0.932
Li et al. [24]	2.434/2.493	1.125/1.098
Chen et al. [25]	1.603/1.831	1.113/1.088
Proposed	1.218/1.226	0.763/0.791

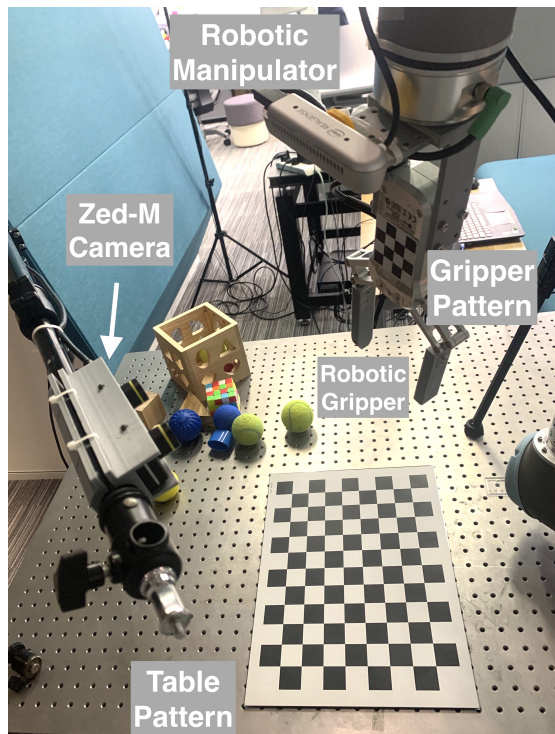


Fig. 6. The experimental platform for dynamic gripper pose tracking.

markers, one may notice that some of them have large bias with respect to the correct corners. The results indicate that the proposed APnP is very accurate and stable. The reason that the accuracies of P3P and EPnP are low is that when the pattern moves, the extracted corner pixels have large errors due to possible motion blur. This can be visualized in the data provided in our open-sourced dataset (see Acknowledgement). The computational efficiency of the proposed APnP is high, since it only requires EIG of a 4x4 matrix, which can be computed instantly via a fast method<sup>4</sup> reported in [14]. Therefore, the designed algorithm can be easily deployed to even low-configuration platforms for accurate camera pose estimation.

### C. Application II: Magnetometer Calibration

For a vector magnetometer, the raw readings can be modeled as

$$\mathbf{m}^b = \mathbf{T}\mathbf{R}\mathbf{m}^r + \mathbf{b}_m + \boldsymbol{\epsilon}_m \quad (44)$$

where  $\mathbf{m}^b$  and  $\mathbf{m}^r$  are 3-D vector measurements of magnetometer in the body frame and reference frame respectively;

<sup>4</sup>[https://github.com/zarathustr/hand\\_eye\\_SO4/blob/master/eig4.m](https://github.com/zarathustr/hand_eye_SO4/blob/master/eig4.m)

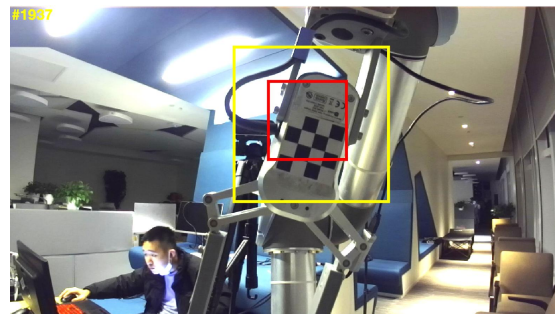


Fig. 7. The tracked chessboard pattern that attached to the robotic gripper. Red: tracked location of pattern; Yellow: Trust region of tracked location.

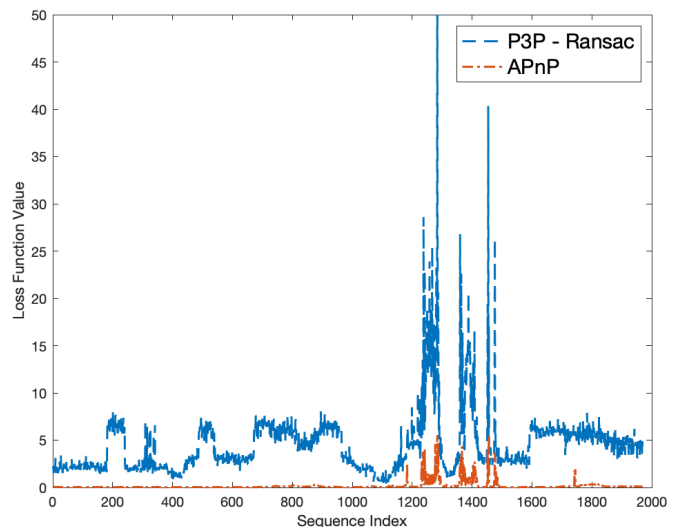


Fig. 8. The comparison of loss function values between P3P (with RANSAC) [16] and the proposed APnP.

$\mathbf{T} \in \mathbb{R}^{3 \times 3}$  stands for the calibration matrix that takes scale factor and nonorthogonality into account;  $\mathbf{R}$  is the rotation matrix in  $SO(3)$ ;  $\mathbf{b}_m$  and  $\boldsymbol{\epsilon}_m \sim \mathcal{N}(\mathbf{0}, \boldsymbol{\Sigma}_{\boldsymbol{\epsilon}_m})$  denote the constant bias and stochastic noise term respectively. The magnetometer calibration problem is to estimate unknown parameters  $\mathbf{T}, \mathbf{R}, \mathbf{b}_m$  and  $\mathbf{m}^r$ , with given measurements of  $\mathbf{m}^b$ . The general calibration problem of magnetometer can be parameterized as follows

$$\begin{aligned} & \arg \min_{\mathbf{T} \in \mathbb{R}^{3 \times 3}, \mathfrak{R} \in SO^{\mathcal{N}}(3), \mathbf{b}_m \in \mathbb{R}^3, \mathbf{m}^r \in \mathbb{R}^3} \sum_{i=1}^{\mathcal{N}} \|\mathbf{m}_i^b - \mathbf{T}\mathbf{R}_i\mathbf{m}^r - \mathbf{b}_m\|^2 \end{aligned} \quad (45)$$

in which  $\mathfrak{R} \in SO^{\mathcal{N}}(3) = SO(3) \times SO(3) \times \dots \times SO(3)$  stands for an element in a power manifold of  $SO(3)$  that includes all  $\mathbf{R}_i$  for  $i = 1, 2, \dots, \mathcal{N}$  with order up to the measurement number  $\mathcal{N}$ , while  $i$  stands for the  $i$ -th sensor sample time instant. (45) is non-convex, NP-hard and usually trivial. As pointed out in [27], (45) suffers from non-unique solutions since  $\mathbf{S}$  and  $\mathbf{R}_i$  are coupled together. Special care has been

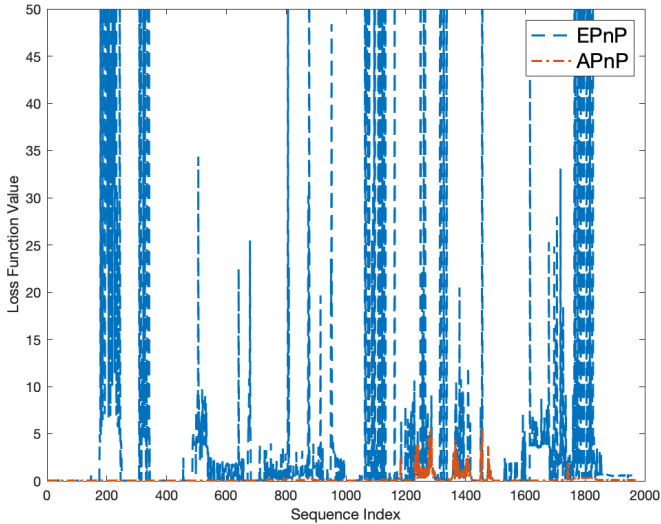


Fig. 9. The comparison of loss function values between EPnP [17] and the proposed APnP.

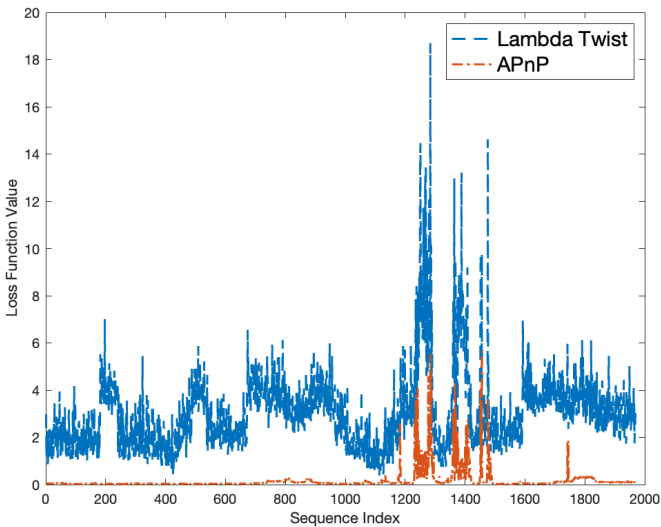


Fig. 10. The comparison of loss function values between Lambda-Twist P3P [32] and the proposed APnP.

taken to relax (45) to

$$\begin{aligned} & \arg \min_{U \in \mathbb{T}(3), \mathbf{b}_m \in \mathbb{R}^3, \tilde{\mathbf{m}}^n \in (\mathbb{U}^3)^{\mathcal{N}}} \sum_{i=1}^{\mathcal{N}} \|\mathbf{m}_i^b - U\tilde{\mathbf{m}}_i^n - \mathbf{b}_m\|^2 \quad (46) \end{aligned}$$

where  $(\mathbb{U}^3)^{\mathcal{N}}$  is the power manifold of unitary 3-D real vector space  $\mathbb{U}^3$  with order  $\mathcal{N}$  so that the  $i$ -th element of  $\mathbf{m}^n$  is  $\mathbf{m}_i^n \in \mathbb{R}^3$ , such that  $\|\mathbf{m}_i^n\| = 1$ ;  $\mathbb{T}(3)$  denotes the group of all real upper triangular matrices. In [27], it has been pointed out that, (46) can be interpreted into another relaxed optimization:

$$\arg \min_{U \in \mathbb{T}(3), \mathbf{b}_m \in \mathbb{R}^3} \sum_{i=1}^{\mathcal{N}} \left(1 - \|\mathbf{U}(\mathbf{m}_i^b - \mathbf{b}_m)\|^2\right)^2 \quad (47)$$

Detailed solutions to (47) have been given in [27], which achieve good accuracy for common datasets. Initial solution to (47) is given by

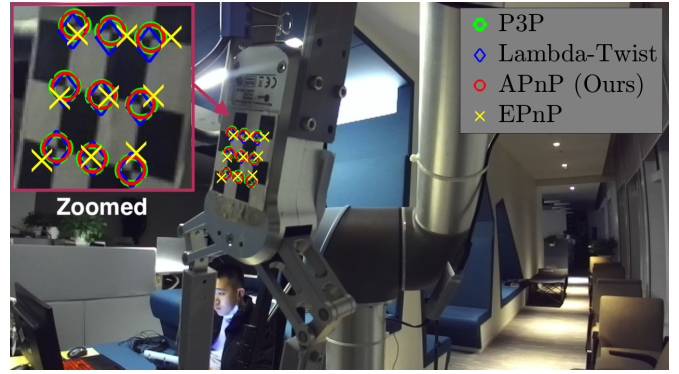


Fig. 11. The visualized reprojected markers using estimated poses from various algorithms.

TABLE III  
ROOT MEAN SQUARED REPROJECTION ERRORS OF MULTIPLE METHODS (IN PIXELS)

Errors	P3P - RANSAC	EPnP	Lambda-Twist P3P	Proposed APnP
X-Axis	2.05076	0.22309	0.87190	<b>0.050636</b>
Y-Axis	2.17841	0.26945	0.86411	<b>0.052172</b>

$\mathbf{z} = \left[ \text{vec}(\mathbf{U}^T \mathbf{U})^T, -2\mathbf{b}_m^T \mathbf{U}^T \mathbf{U}, \mathbf{b}_m^T \mathbf{U}^T \mathbf{U} \mathbf{b}_m - 1 \right]^T$ , such that

$$\mathbf{Y} \mathbf{z} = 0 \quad (48)$$

where  $\mathbf{Y}$  is determined by measurements  $\mathbf{m}_i^b$  for  $i = 1, 2, \dots, \mathcal{N}$ . Solution of  $\mathbf{z}$  can be sought by SVD of  $\mathbf{Y}$  or EIG of  $\mathbf{Y}^T \mathbf{Y}$ . However, when there are many outliers or insufficient measurements, the optimization can hardly be performed. From (48), it is able for us to see that since  $\mathbf{z} \in \mathbb{R}^{10}$ , at least 10 non-coplanar measurements are required to obtain the initial solution. If the outlier rate is high or the measurements are not sufficient, the linear system (48) will become ill-posed, that is,  $\mathbf{U}^T \mathbf{U}$  in  $\mathbf{z}$  cannot be guaranteed to be positive semidefinite. In this case, there is no such a Cholesky decomposition for a non-positive semidefinite matrix. The origin of (47) is that, for ideal measurements, one has

$$\|\mathbf{U}(\mathbf{m}_i^b - \mathbf{b}_m)\| = 1 \quad (49)$$

Expanding (49), we have

$$(\mathbf{m}_i^b - \mathbf{b}_m)^T \mathbf{U}^T \mathbf{U} (\mathbf{m}_i^b - \mathbf{b}_m) = 1 \quad (50)$$

Let  $\mathbf{V}^T \mathbf{D} \mathbf{V} = \mathbf{U}^T \mathbf{U}$  be an SO(3) eigen-decomposition (SO(3)-EIG) of  $\mathbf{U}^T \mathbf{U}$  such that  $\mathbf{D}$  denotes the matrix with diagonal entries of eigenvalues and  $\mathbf{V} \in \text{SO}(3)$  is the orthonormal basis of  $\mathbf{U}^T \mathbf{U}$ . The SO(3)-EIG is not difficult since for one matrix  $\mathbf{X}$  if  $\mathbf{W}^T \mathbf{D} \mathbf{W} = \mathbf{X}$ , where  $\det(\mathbf{W}) = -1$ ,  $\mathbf{V}^T \mathbf{D} \mathbf{V} = \mathbf{X}$  also holds for  $\mathbf{V} = -\mathbf{W} \in \text{SO}(3)$ . Then, (50) denotes an ellipsoid such that the center is  $\mathbf{b}_m$  and the semi-major axes are determined by the square roots of the diagonal elements in the inverse of  $\mathbf{D}$ . (50) can be further explicitly given as

$$(\mathbf{m}_i^b - \mathbf{b}_m)^T \mathbf{V}^T \mathbf{D} \mathbf{V} (\mathbf{m}_i^b - \mathbf{b}_m) = 1 \quad (51)$$

which can be treated as a unit sphere, say  $\mathcal{X}$ ,

$$\mathcal{X} : \mathbf{x}^\top \mathbf{x} = 1 \quad (52)$$

that is located in the origin by substitution of  $\mathbf{x} = \pm\sqrt{\mathbf{D}}\mathbf{V}(\mathbf{m}_i^b - \mathbf{b}_m)$ . Therefore (47) is actually an ellipsoid fitting problem and need not to be solved in the way of (48). For the model (51), we have 9-degree of freedom for the unknowns, which is less than the number of unknowns in (48). The vector-field sensor intrinsic calibration problem turns into a surface registration problem with scale of  $\mathcal{K} = \sqrt{\mathbf{D}} \in \text{diag}(\mathbb{R}_+^3)$ , rotation of  $\mathbf{R} = \mathbf{V} \in \text{SO}(3)$  and translation of  $\mathbf{t} = -\mathcal{K}\mathbf{V}\mathbf{b}_m \in \mathbb{R}^3$ , such that we find a rigid transformation that satisfies

$$\mathbf{x}_i = \mathcal{K}\mathbf{R}\mathbf{m}_i^b + \mathbf{t} \quad (53)$$

in which  $\mathbf{v}_i^b$  on the ellipsoid surface is the  $i$ -th corresponding point of  $\mathbf{x}_i$  on the unit sphere (52), given by raw measurements  $\mathbf{v}_i^b$  for  $i = 1, 2, \dots, \mathcal{N}$ . Sometimes, when the three axes of magnetometer are isotropic,  $\mathcal{K}$  becomes a scalar, say  $s$ , such that  $\mathbf{x}_i = s\mathbf{R}\mathbf{v}_i^b + \mathbf{t}$  and  $s$  actually represents the magnitude of the geomagnetic field at the local geodetic coordinates. The new problem is challenging, that is, it is now being formulated as a point-surface registration. We now solve it in a new geometrical manner. The point-surface registration is based on a fact that the geometry of the optimal surface formed by the points is homotopic to the surface to be registered. Note that here, homotopy is not rigorously identical to homeomorphism since the two registered surfaces do not always maintain the same inner volume. Therefore we solve the problem in a discrete way. The following criteria has been proposed

$$\begin{aligned} \arg \min_{\mathbf{R} \in \text{SO}(3)} \quad & \arg \max_{\mathbf{r}_j \in \mathcal{X}} \sum \| \mathbf{r}_j - \mathcal{K}\mathbf{R}\mathbf{p}_j + \mathbf{t} \|^2 \\ \mathbf{t} \in \mathbb{R}^3 \quad & \mathbf{p}_j \in \tilde{\mathcal{Y}} \subset \mathcal{Y} \\ \mathcal{K} \in \text{diag}(\mathbb{R}_+^3) \end{aligned} \quad (54)$$

The inner optimization maximizes the count of the points by selecting the most appropriate subset  $\tilde{\mathcal{Y}}$  of the measurement set  $\mathcal{Y}$ , which forms an ellipsoidal surface that corresponds to the unit sphere  $\mathcal{X}$ . The outer optimizer then minimizes the objective function subject to the rigid loss defined in (53). In the inner loop, once a temporary  $\tilde{\mathcal{Y}}$  has been found, the ellipsoid equation can be fitted via (51) and thus a rough guess of  $s$ ,  $\mathbf{R}$  and  $\mathbf{t}$  can be obtained. Then, via  $s$ ,  $\mathbf{R}$  and  $\mathbf{t}$ , the entire measurement set  $\mathcal{Y}$  can be remapped to fit the unit sphere  $\mathcal{X}$ . In this way, by Cartesian distances of the remapped points to the unit surface, we can select best points that are closest to  $\mathcal{X}$ . This results in a new map from  $\mathcal{X}$  back to  $\mathcal{Y}$ , that recursively refines the two surfaces, which we name it for the first time, as the iterative closest points and surfaces (ICPS). The kernel of this problem is solved via the proposed solver from (23) to (38).

To verify the proposed algorithm, we first conduct a hardware-in-the-loop (HITL) simulation. The 3DM-GX5-25 from Microstrain Inc. is employed to collect reference attitude information and calibrated magnetometer readings (see Fig. 12). The data is gathered at the frequency of 100Hz. Then, the reference attitude matrices and magnetic data are utilized for simulation of distorted magnetic readings, including

anisotropic scale factor and bias. The distorted magnetometer data will be calibrated using the proposed method and the 3-D results are shown in Fig. 13. The magnetic norms before and after the calibration are shown in Fig. 14.



Fig. 12. The 3DM-GX5-25 inertial measurement unit for hardware-in-the-loop simulation.

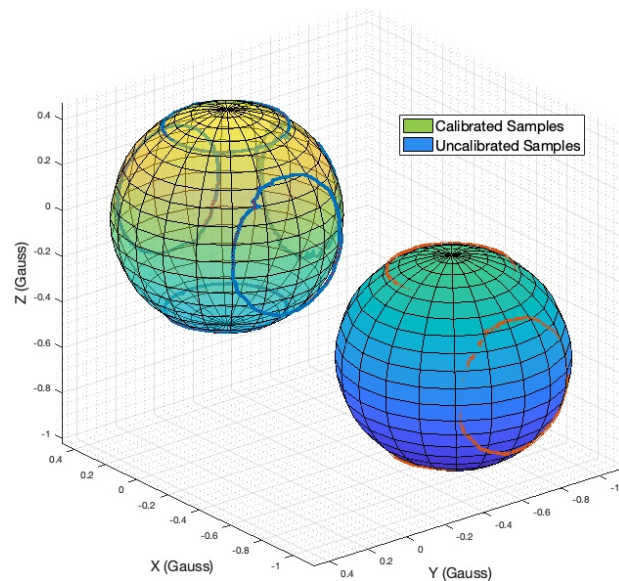


Fig. 13. Calibration results using the proposed method.

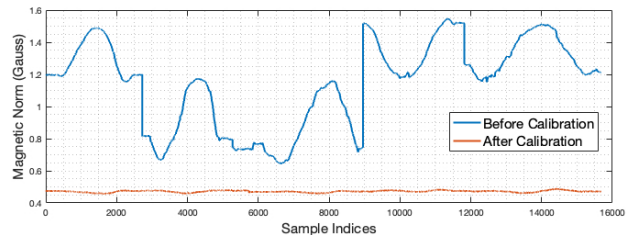


Fig. 14. Magnetic norm before/after calibration using the proposed method.

We compare the proposed method with two previous method by Wu et al. [27] and Vasconcelos et al. [36]. After calibration, the calibration results from various methods are placed into a

Kalman filter for attitude estimation from inertial and magnetic measurements [37]. During the HITL simulation, different outlier ratios are simulated. The results are shown in Table IV. The attitude errors are evaluated by the norm of the angle axis (Rodrigues vector) of the estimated attitude matrix and reference one.

TABLE IV  
ROOT MEAN SQUARED ATTITUDE ERRORS AFTER MAGNETOMETER CALIBRATION SUBJECT TO DIFFERENT OUTLIER RATIOS (IN DEGREE)

Outlier	Wu et al. [27]	Vasconcelos et al. [36]	Proposed
5%	0.54906	0.82433	<b>0.37805</b>
10%	2.34245	4.32126	<b>1.17829</b>
20%	6.57822	10.33268	<b>2.21061</b>

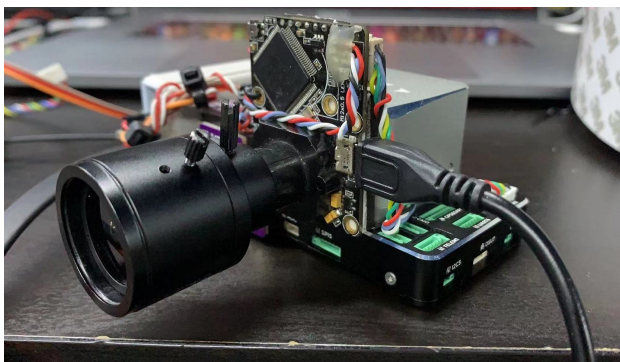


Fig. 15. The designed inertial/magnetic/visual odometry system.

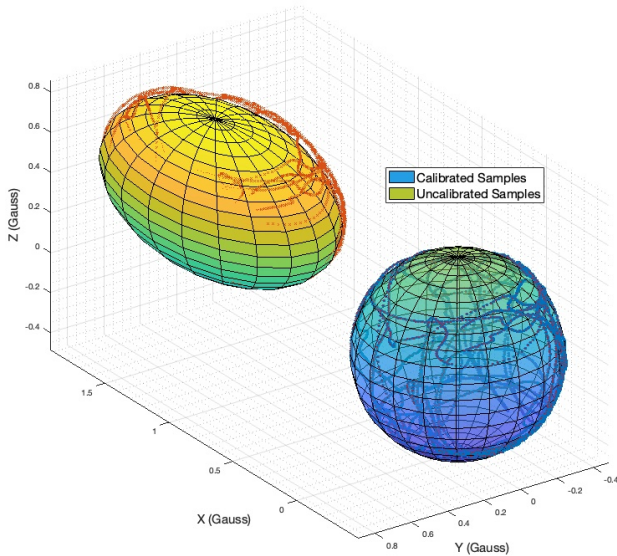


Fig. 16. The magnetometer calibration results of the designed odometry system.

The results indicate that the proposed method outperforms these representative candidates. The main advantage is that the proposed method is able to estimate robust magnetometer calibration parameters subject to high outlier ratios, which indirectly verifies the effectiveness of the proposed solution to anisotropic-scale registration problem. Moreover, the designed

method is brought to our designed inertial/magnetic/visual odometry system. This system employs a magnetometer of RM3110, an inertial measurement unit (IMU) of ICM20948 and a global-shutter camera of MT9V034. The camera sensor needs much more power when capturing images than other inertial and magnetic sensors. This will cause sudden electromagnetic disturbances in the magnetic readings. Traditional methods like [27] and [36] cannot deal with the calibration problem very effectively for such a system. We use our proposed method to estimate the magnetic calibration parameters via (54). One of the many results will be presented in Fig. 16. Using the calibration results, we are able to compensate for the fast camera motion distortion by magnetometer. The attitude estimation accuracy of the results with our calibration is 0.5203 degree in average for Euler angles and is 0.9811 degree with the method in [27], which verifies the superiority of our approach.

TABLE V  
TIME EFFICIENCY PROFILES OF VARIOUS ANISOTROPIC REGISTRATION METHODS (IN SECONDS)

Du et al. [23]	Li et al. [24]	Chen et al. [25]	Proposed
0.0923	0.0798	0.1247	0.0712

TABLE VI  
TIME EFFICIENCY PROFILES OF VARIOUS PNP METHODS (IN SECONDS)

P3P - RANSAC [16]	EPnP [17]	Lambda-Twist P3P [32]	Proposed APnP
0.00285	0.00464	0.01832	0.00403

#### D. Time Efficiency

Time efficiency plays a vital role in perspective-n-points, point cloud registration, and magnetometer calibration, as these processes often deal with vast amounts of data and require real-time performance. In perspective-n-points, efficient algorithms for feature extraction, correspondence matching, and pose estimation are essential to ensure swift and accurate computation of camera pose from 2D-3D correspondences. Similarly, point cloud registration relies on optimized submodules for keypoint detection, feature description, and transformation estimation to quickly align and fuse multiple point clouds into a coherent 3D model. Magnetometer calibration also demands time-efficient techniques for data collection, noise filtering, and parameter estimation to promptly compensate for sensor errors and ensure precise orientation tracking. By prioritizing time efficiency and optimizing submodules, these processes can deliver high-quality results with minimal latency, enabling their effective deployment in various applications such as augmented reality, autonomous navigation, and geospatial mapping. Through previous experimental validations, we also test the time efficiency of various algorithms. Specifically, we summarize the results in Table V, VI, VII.

In each test, we test various candidates for 1000 times to get the average time efficiency profiles. The time efficiency evaluation has been conducted on a machine with i7-8500

TABLE VII  
 TIME EFFICIENCY PROFILES OF VARIOUS MAGNETOMETER CALIBRATION  
 METHODS (IN SECONDS)

Wu et al. [27]	Vasconcelos et al. [36]	Proposed
0.6436	0.7689	0.9892

central processing unit, 16GB RAM and 1TB SSD disk storage. Seen from the tables, it is found out that the proposed method has better time efficiency than other methods in 3-D registration and PnP tasks. However, it is notable that in magnetometer calibration tasks, the proposed method is slower than the existing representatives. This is because the proposed one requires more iterations to achieve good inlier estimation over large datasets while the kernel computation module, being anisotropic, indeed requires higher computational burden than those analytical guesses in existing works. Therefore there is a trade-off between the time efficiency and accuracy for the sensor calibration tasks. For other tasks, the proposed method maintains faster than representatives.

## V. CONCLUSION

After revisiting traditional similarity transformation problems, we prove that two representative branches, i.e., scale-stretching point-cloud registration and perspective-n-points, can be solved in a unified manner. Furthermore, it is shown that an extended anisotropic-scale problem is challenging and detailed globally optimal solutions are derived to solve this problem. The developed approach has been successfully applied to industrial robotic grasping tasks and magnetometer calibration. Future efforts will be paid to finding more potentially better solutions to these problems. Partial experimental data and codes of this paper are open-source at <https://github.com/zarathustr/APnP>.

## ACKNOWLEDGEMENT

This work has been supported by Robotics Institute, Hong Kong University of Science and Technology, under the administration of Prof. F. Zhang.

## REFERENCES

- [1] Z. Min, J. Wang, and M. Q. Meng, "Robust Generalized Point Cloud Registration with Orientational Data Based on Expectation Maximization," *IEEE Trans. Autom. Sci. Eng.*, vol. 17, no. 1, pp. 207–221, 2020.
- [2] Z. Min, H. Ren, and M. Q. Meng, "Statistical Model of Total Target Registration Error in Image-Guided Surgery," *IEEE Trans. Autom. Sci. Eng.*, vol. 17, no. 1, pp. 151–165, 2020.
- [3] J. Wu, Y. Sun, M. Wang, and M. Liu, "Hand-eye calibration: 4-d procrustes analysis approach," *IEEE Trans. Instrum. Meas.*, vol. 69, no. 6, pp. 2966–2981, 2019.
- [4] S. Qiu, M. Wang, and M. R. Kermani, "A new formulation for hand-eye calibrations as point-set matching," *IEEE Trans. Instrum. Meas.*, vol. 69, no. 9, pp. 6490–6498, 2020.
- [5] F. L. Markley, "Attitude Determination using Vector Observations and the Singular Value Decomposition," *J. Astronaut. Sci.*, vol. 36, no. 3, pp. 245–258, 1987.
- [6] K. S. Arun, T. S. Huang, and S. D. Blostein, "Least-Squares Fitting of Two 3-D Point Sets," *IEEE Trans. Pattern Anal. Mach. Intell.*, vol. PAMI-9, no. 5, pp. 698–700, 1987.

- [7] P. J. Besl and N. D. McKay, "A Method for Registration of 3-D Shapes," *IEEE Trans. Pattern Anal. Mach. Intell.*, vol. 14, no. 2, pp. 239–256, 1992.
- [8] Z. Zhang, "Iterative point matching for registration of free-form curves and surfaces," *Int. J. Comput. Vis.*, vol. 13, no. 2, pp. 119–152, 1994.
- [9] J. Wu, "Rigid 3D Registration: A Simple Method Free of SVD and Eigen-Decomposition," *IEEE Trans. Instrum. Meas.*, vol. 16, no. 18, pp. 6997–7007, 2020.
- [10] B. K. P. Horn, "Closed-form solution of absolute orientation using unit quaternions," *J. Opt. Soc. Am. A*, vol. 4, no. 4, p. 629, 1987.
- [11] B. K. P. Horn, H. M. Hilden, and S. Negahdaripour, "Closed-form solution of absolute orientation using orthonormal matrices," *J. Opt. Soc. Am. A*, vol. 5, no. 7, p. 1127, 1988.
- [12] S. Ying, J. Peng, S. Du, and H. Qiao, "A scale stretch method based on ICP for 3D data registration," *IEEE Trans. Autom. Sci. Eng.*, vol. 6, no. 3, pp. 559–565, 2009.
- [13] L. Quan and Z. Lan, "Linear N-point camera pose determination," *IEEE Trans. Pattern Anal. Mach. Intell.*, vol. 21, no. 8, pp. 774–780, 1999.
- [14] J. Wu, M. Liu, Z. Zhou, and R. Li, "Fast Symbolic 3-D Registration Solution," *IEEE Trans. Autom. Sci. Eng.*, vol. 17, no. 2, pp. 761–770, 2020.
- [15] S. Sarabandi, A. Shabani, J. M. Porta, and F. Thomas, "On Closed-Form Formulas for the 3-D Nearest Rotation Matrix Problem," *IEEE Trans. Robot.*, vol. 36, no. 4, pp. 1333–1339, 2020.
- [16] X.-S. Gao, X.-R. Hou, J. Tang, and H.-f. Cheng, "Complete Solution Classification for the Perspective-Three-Point Problem," *IEEE Trans. Pattern Anal. Mach. Intell.*, vol. 25, no. 8, pp. 930–943, 2003.
- [17] V. Lepetit, F. Moreno-Noguer, and P. Fua, "EPnP: An accurate O(n) solution to the PnP problem," *Int. J. Comput. Vis.*, vol. 81, no. 2, pp. 155–166, 2009.
- [18] D. Grant, J. Bethel, and M. Crawford, "Point-to-plane registration of terrestrial laser scans," *ISPRS J. Photogramm. Remote Sens.*, vol. 72, pp. 16–26, 2012. [Online]. Available: <http://dx.doi.org/10.1016/j.isprsjprs.2012.05.007>
- [19] Y. Pan, P. Xiao, Y. He, Z. Shao, and Z. Li, "Mulls: Versatile lidar slam via multi-metric linear least square," *arXiv preprint arXiv:2102.03771*, 2021.
- [20] S. Li, C. Xu, and M. Xie, "A Robust O(n) Solution to the Perspective-n-Point Problem," *IEEE Trans. Pattern Anal. Mach. Intell.*, vol. 34, no. 7, pp. 1444–1450, 2012.
- [21] C. Xu, L. Zhang, L. Cheng, and R. Koch, "Pose Estimation from Line Correspondences: A Complete Analysis and a Series of Solutions," *IEEE Trans. Pattern Anal. Mach. Intell.*, vol. 39, no. 6, pp. 1209–1222, 2017.
- [22] Z. Min, J. Wang, J. Pan, and M. Q. Meng, "Generalized 3-D Point Set Registration With Hybrid Mixture Models for Computer-Assisted Orthopedic Surgery: From Isotropic to Anisotropic Positional Error," *IEEE Trans. Autom. Sci. Eng.*, pp. 1–13, 2020.
- [23] S. Du, N. Zheng, L. Xiong, S. Ying, and J. Xue, "Scaling iterative closest point algorithm for registration of m-d point sets," *J. Vis. Comm. Image Represent.*, vol. 21, no. 5-6, pp. 442–452, 2010.
- [24] W.-L. Li, H. Xie, Z.-P. Yin, and Y.-L. Xiong, "A new algorithm for non-rigid shape matching with anisotropic-scaling transformation parameters," *Int. J. Precis. Eng. Manufact.*, vol. 16, pp. 895–903, 2015.
- [25] E. C. Chen, A. J. McLeod, J. S. Baxter, and T. M. Peters, "Registration of 3d shapes under anisotropic scaling: anisotropic-scaled iterative closest point algorithm," *Int. J. Comput. Assist. Radio. Surgery*, vol. 10, pp. 867–878, 2015.
- [26] V. Garro, F. Crosilla, and A. Fusiello, "Solving the pnp problem with anisotropic orthogonal procrustes analysis," in *2012 Second International Conference on 3D Imaging, Modeling, Processing, Visualization & Transmission*. IEEE, 2012, pp. 262–269.
- [27] Y. Wu and W. Shi, "On Calibration of Three-Axis Magnetometer," *IEEE Sens. J.*, vol. 15, no. 11, pp. 6424–6431, 2015.
- [28] I. Y. Bar-Itzhack, "New Method for Extracting the Quaternion from a Rotation Matrix," *Journal of Guidance, Control, and Dynamics*, vol. 23, no. 6, pp. 1085–1087, 2000.
- [29] J. Wu, Z. Zhou, J. Chen, H. Fourati, and R. Li, "Fast Complementary Filter for Attitude Estimation Using Low-Cost MARG Sensors," *IEEE Sens. J.*, vol. 16, no. 18, pp. 6997–7007, 2016.
- [30] J. Wu, Z. Zhou, B. Gao, R. Li, Y. Cheng, and H. Fourati, "Fast Linear Quaternion Attitude Estimator Using Vector Observations," *IEEE Trans. Autom. Sci. Eng.*, vol. 15, no. 1, pp. 307–319, 2018.
- [31] G. Turk and M. Levoy, "Zippered polygon meshes from range images," in *Proceedings of the 21st annual conference on Computer graphics and interactive techniques*, 1994, pp. 311–318.

- [32] M. Persson and K. Nordberg, "Lambda twist: An accurate fast robust perspective three point (p3p) solver," in *ECCV 2018*, V. Ferrari, M. Hebert, C. Sminchisescu, and Y. Weiss, Eds. Cham: Springer International Publishing, 2018, pp. 334–349.
- [33] Z. Zhang, "A Flexible New Technique for Camera Calibration," *IEEE Trans. Pattern Anal. Mach. Intell.*, vol. 22, no. 11, pp. 1330–1334, 2000.
- [34] A. Geiger, F. Moosmann, Ö. Car, and B. Schuster, "Automatic camera and range sensor calibration using a single shot," *Proc. - IEEE Int. Conf. Robot. Autom.*, pp. 3936–3943, 2012.
- [35] K. Zhang, L. Zhang, and M. H. Yang, "Fast Compressive Tracking," *IEEE Trans. Pattern Anal. Mach. Intell.*, vol. 36, no. 10, pp. 2002–2015, 2014.
- [36] J. F. Vasconcelos, G. Elkaim, C. Silvestre, P. Oliveira, and B. Cardeira, "Geometric approach to strapdown magnetometer calibration in sensor frame," *IEEE Trans. Aerosp. Electron. Syst.*, vol. 47, no. 2, pp. 1293–1306, 2011.
- [37] J. Wu, "MARG Attitude Estimation Using Gradient-Descent Linear Kalman Filter," *IEEE Trans. Autom. Sci. Eng.*, vol. 17, no. 4, pp. 1777–1790, 2020.



**Jin Wu** (Member, IEEE) received a B.S. degree from the University of Electronic Science and Technology of China, Chengdu, China. From 2013 to 2014, he was a visiting student with Groep T, Katholieke Universiteit Leuven (KU Leuven). He is currently pursuing a Ph.D. degree in the Department of Electronic and Computer Engineering, Hong Kong University of Science and Technology (HKUST), Hong Kong, supervised by Prof. Wei Zhang. He was awarded the outstanding reviewer of IEEE TRANSACTIONS ON INSTRUMENTATION

AND MEASUREMENT in 2021. He is now a review editor of *Frontiers in Aerospace Engineering* and an invited guest editor for several JCR-indexed journals. He is also an IEEE Consumer Technology Society (CTSoc) member and a committee member and publication liaison. He was a committee member for the IEEE CoDIT in 2019, a special section chair for the IEEE ICGNC in 2021, a special session chair for the 2023 IEEE ITSC, a track chair for the 2024 IEEE ICCE, 2024 IEEE ICCE-TW and a chair for the 2024 IEEE GEM conferences. From 2019 to 2020, he was with Tencent Robotics X, Shenzhen, China. He was selected as the World's Top 2% Scientist by Stanford University and Elsevier in 2020, 2021 and 2022. His research falls within the algorithmic foundations for robotics with particular focuses on attitude/pose estimation and related mechatronic systems design/control, numerical optimization, deep learning, and high-performance computing, with applications in aerospace engineering, space sciences, industrial/mobile robotics, computer vision, structural chemistry, computer animation, and consumer electronics



**Chaoqun Wang** (Member, IEEE) received the B.E. degree in automation from Shandong University, Jinan, China, in 2014, and the Ph.D. degree in robot and artificial intelligence from the Department of Electronic Engineering, The Chinese University of Hong Kong, Hong Kong, in 2019.

During the Ph.D. study, he spent six months with The University of British Columbia, Vancouver, BC, Canada, as a Visiting Scholar. From 2019 to 2020, he was a Post-Doctoral Fellow with the Department of Electronic Engineering, The Chinese University of

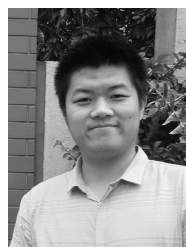
Hong Kong. He is currently a Professor with the School of Control Science and Engineering, Shandong University. His current research interests include autonomous vehicles, active and autonomous exploration, and path planning.



**Chong Li** (S'15-M'17) received his B.S. and M.S. in Automation and Control Theory & Engineering, from Ocean University of China, Qingdao, China, in 2009 and 2012, respectively. He received his Ph.D in Mechanical Engineering, from Auburn University, Auburn, AL, United States, in 2016. Then he joined iMEMS Lab at Georgia Tech as a postdoctoral research fellow from 2016 to 2018.

Currently, Dr. Chong Li is a Professor with Department of Automation & Measurement, Ocean University of China. His research interests include

precision control systems, resonant gyroscopes, navigation & guidance, and instrumentation technology.



**Yi Jiang** (Member, IEEE) received the B.Eng. degree in automation, M.S. and Ph.D. degrees in control theory and control engineering from Information Science and Engineering College and State Key Laboratory of Synthetical Automation for Process Industries in Northeastern University, Shenyang, Liaoning, China in 2014, 2016 and 2020, respectively.

From January to July 2017, he was a Visiting Scholar with the UTA Research Institute, University of Texas at Arlington, TX, USA, and from March 2018 to March 2019, he was a Research Assistant

with the University of Alberta, Edmonton, Canada. Currently, he is a Postdoc Fellow with the City University of Hong Kong, Hong Kong. His research interests include networked control systems, industrial process operational control, reinforcement learning and event-triggered control. Dr. Jiang is an Associate Editor for *Advanced Control for Applications: Engineering and Industrial Systems*, and the recipient of Excellent Doctoral Dissertation Award from Chinese Association of Automation (CAA) in 2021 and Hong Kong Research Grants Council (RGC) Postdoctoral Fellowship Scheme (PDFS) 2023/24.



**Chengxi Zhang** (Member, IEEE) received B.S. and M.S. degrees from Harbin Institute of Technology, China, in 2012 and 2015; and Ph.D. degree from Shanghai Jiao Tong University, China, in 2019. He is now an Associate Professor at Jiangnan University, China. His interests are space engineering, robotic systems & control. He is an Invited Session Chair of JACA2022, Wuxi; CCDC2024, Xi'an; FASTA2024, Shenzhen; Technical Program Committee of IEEE GEM 2024, Turin. He is an Associate Editor of *Frontiers in Aerospace Engineering*, on Editorial Board

of *IoT, AppliedMath, Complex Engineering Systems, AI and Autonomous Systems, Aerospace Systems, and Astrodynamics*.



**Yulong Huang** received the B.S. degree in Automation from the College of Automation, Harbin Engineering University, Harbin, China, in 2012. He received the Ph.D. degree in control science and engineering from the College of Automation, Harbin Engineering University, Harbin, China, in 2018. From Nov. 2016 to Nov. 2017, he was a visiting graduate researcher at the Electrical Engineering Department of Columbia University, New York, USA. From Dec. 2019 to Dec. 2021, he was associated with the Department of Mechanical Engineering,

City University of Hong Kong, as a Hong Kong Scholar.

He is a Full Professor of navigation, guidance, and control, and Vice Dean of College of Intelligent Systems Science and Engineering at Harbin Engineering University (HEU) in China. His current research interests include state estimation, intelligent information fusion and their applications in navigation technology, such as inertial navigation, integrated navigation, intelligent navigation, and cooperative navigation. Currently, he serves as an Associate Editor for the IEEE TRANSACTIONS ON AEROSPACE AND ELECTRONIC SYSTEMS, for the IEEE TRANSACTIONS ON INSTRUMENTATION AND MEASUREMENT, and for the IEEE SENSORS JOURNAL, and a Youth Editor for the IEEE/CAA JOURNAL OF AUTOMATICA SINICA (JAS).

He was the recipient of the 2018 IEEE Barry Carlton Award from IEEE TRANSACTIONS ON AEROSPACE AND ELECTRONIC SYSTEMS in 2022, the Honorable Mention of 2017 IEEE Barry Carlton Award from IEEE TRANSACTIONS ON AEROSPACE AND ELECTRONIC SYSTEMS in 2021, the Best Student Paper Award of 2023 IEEE International Conference on Mechatronics and Automation (IEEE ICMA 2023), and the Best Paper Award of 2021 International Conference on Autonomous Unmanned Systems (ICAUS 2021). He was also the recipient of the 11th China Youth Science and Technology Innovation Awards in 2018, the excellent doctoral thesis from Chinese Association of Automation (CAA) in 2019, the Wu WenJun AI Excellent Youth Scholar Award in 2021, the First Prize of Natural Science Award of Chinese Association of Automation (Ranked the 2nd) in 2021, and he was selected into the sixth Young Elite Scientists Sponsorship Program by China Association for Science and Technology in 2020. He was an outstanding Associate Editor and Reviewer for the IEEE TRANSACTIONS ON INSTRUMENTATION AND MEASUREMENT.



**Yuhua Qi** received the B.S. and Ph.D. degrees in aerospace engineering from the Beijing Institute of Technology, Beijing, China, in 2020.

He is currently a Postdoctoral Researcher at the School of Systems Science and Engineering, Sun Yat-sen University, Guangzhou, China. His research interests include multirobot simultaneous localization and mapping (SLAM), cooperative control, and autonomous unmanned systems.



**Bohuan Xue** received the B.Eng. degree in computer science and technology from the College of Mobile Telecommunications, Chongqing University of Posts and Telecommunications, Chongqing, China, in 2018. He is currently pursuing the Ph.D. degree in electrical engineering with the Department of Computer Science and Engineering, Hong Kong University of Science and Technology, Hong Kong, SAR, China. His research interests include simultaneous localization and mapping (SLAM), computer vision, and 3-D reconstruction.



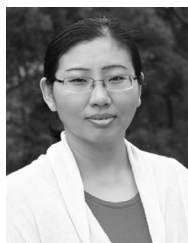
**Jianhao Jiao** (Member, IEEE) was born in 1994. He received the B.Eng. degree in instrument science from Zhejiang University, Hangzhou, China, in 2017, and the Ph.D. from the Department of Electronic and Computer Engineering, the Hong Kong University of Science and Technology, Hong Kong, China, in 2021. He is currently with Department of Computer Science, University College London, as a Senior Research Fellow, in collaboration with Prof. Dimitrios Kanoulas.

His research interests include state estimation, SLAM, sensor fusion, and computer vision. He has published his research works in top robotics venues including IEEE TRANSACTIONS ON ROBOTICS, ICRA, and IROS. He is a reviewer of IEEE TRANSACTIONS ON ROBOTICS and an Associate Editor for IEEE IROS 2024.



**Rui Fan** received a B.Eng. degree in automation from the Harbin Institute of Technology in 2015 and a Ph.D. degree (supervisors: Prof. John G. Rarity and Prof. Naim Dahnoun) in Electrical and Electronic Engineering from the University of Bristol in 2018. He worked as a research associate (supervisor: Prof. Ming Liu) at the Hong Kong University of Science and Technology from 2018 to 2020 and a postdoctoral scholar-employee (supervisors: Prof. Linda M. Zangwill and Prof. David J. Kriegman) at the University of California San Diego between 2020 and 2021. He began his faculty career as a full research professor with the College of Electronics & Information Engineering at Tongji University in 2021 and was then promoted to a full professor in the same college and at the Shanghai Research Institute for Intelligent Autonomous Systems in 2022.

Prof. Fan served as an associate editor for ICRA'23 and IROS'23/24, an Area Chair for ICIP'24, and a senior program committee member for AAAI'23/24. He is the general chair of the AVVision community and has organized several impactful workshops and special sessions in conjunction with WACV'21, ICIP'21/22/23, ICCV'21, and ECCV'22. He was honored by being included in the Stanford University List of Top 2% Scientists Worldwide in both 2022 and 2023, recognized on the Forbes China List of 100 Outstanding Overseas Returnees in 2023, and acknowledged as one of Xiaomi Young Talents in 2023. His research interests include computer vision, deep learning, and robotics.



**Wei Zhang** is a Professor with the Department of Electronic and Computer Engineering, the Hong Kong University of Science and Technology (HKUST). She received her Ph.D. degree in Electrical Engineering from Princeton University with Wu Prize for research excellence. She was an Assistant Professor with the School of Computer Engineering, Nanyang Technological University, Singapore, from 2010 to 2013. She was a co-investigator of Singapore-MIT Alliance for Research and Technology, and a collaborator of ASTAR-UIUC Advanced

Digital Sciences Center. She joined HKUST in 2013 and established Reconfigurable Computing Systems Lab. She has authored over 100 technical papers in referred international journals and conferences and authored three book chapters. Her team has won the best paper award in ISVLSI 2009, ICCAD 2017, and ICCAD 2022.

Prof. Zhang currently serves in several editorial boards as Associate Editor including IEEE TRANSACTIONS ON VERY LARGE SCALE INTEGRATION SYSTEMS, IEEE TRANSACTIONS ON COMPUTER-AIDED DESIGN OF INTEGRATED CIRCUITS AND SYSTEMS, *ACM Transactions on Embedded Computing Systems*, *ACM Journal on Emerging Technologies in Computing Systems* and *ACM Transactions on Reconfigurable Technology and Systems*. She also serves on many organization committees and technical program committees, such as DAC, ICCAD, CASES, FPGA, FCCM, etc. Prof. Zhang's current research interests include reconfigurable systems, FPGA-based design, low-power high-performance multicore systems, electronic design automation, embedded systems, and emerging technologies.